Rate Splitting for Uplink NOMA With Enhanced Fairness and Outage Performance

Article *in* IEEE Transactions on Wireless Communications · March 2020

DOI: 10.1109/TWC.2020.2985970

CITATIONS
62

READS
585

5 authors, including:

Hongwu Liu
Shandong Jiaotong University
114 PUBLICATIONS **721** CITATIONS
SEE PROFILE

Theodoros Tsiftsis
University of Thessaly
340 PUBLICATIONS **9,725** CITATIONS
SEE PROFILE

Kyeong Jin Kim
Samsung Research America (SRA)
246 PUBLICATIONS **3,096** CITATIONS
SEE PROFILE

Kyung Sup Kwak
Inha University
902 PUBLICATIONS **15,939** CITATIONS
SEE PROFILE

Rate Splitting for Uplink NOMA with Enhanced Fairness and Outage Performance

Hongwu Liu, *Senior Member, IEEE,* Theodoros A. Tsiftsis, *Senior Member, IEEE,*
Kyeong Jin Kim, *Senior Member, IEEE,* Kyung Sup Kwak, *Member, IEEE,*
and H. Vincent Poor, *Life Fellow, IEEE*

***Abstract*—In this paper, we investigate rate splitting (RS) for an uplink non-orthogonal multiple access (NOMA) system with a pair of near and far users adopting cyclic prefixed single carrier transmissions. Frequency-domain equalization is applied to assist successive interference cancellation at the base-station. Two kinds of RS schemes, namely, fixed RS (FRS) and cognitive RS (CRS) schemes, are proposed to realize RS for uplink NOMA with the aim of improving user fairness and outage performance in delay-limited transmissions. Corresponding to the split data streams, transmit power is allocated in either fixed or cognitive manner for the FRS and CRS schemes, respectively. Based on achievable rate region analysis, the benefits of applying RS to uplink NOMA for enhancing the user fairness and outage performance are revealed. A modified Jain's index is proposed to measure the user fairness for the considered delay-limited transmissions. Closed-form expressions are derived for the outage probabilities of the paired users, respectively, whereas the preferred system parameters are chosen based on asymptotic outage probability expressions. The enhanced user fairness and superior outage performance of the proposed RS schemes are corroborated by Monte Carlo simulation results.**

***Index Terms*—NOMA, rate splitting (RS), user fairness, outage probability.**

I. Introduction

As a promising radio access technology to meet demands for spectrally-efficient massive connectivity, non-orthogonal multiple access (NOMA) has gained tremendous attention from academia and industry [2]–[4]. Sharing the same time/frequency/code resource block, signals of multiple users are superimposed in the power-domain and successive interference cancellation (SIC) is adopted at the receiver side in NOMA systems, which offer superior spectral efficiency and user fairness over those of conventional orthogonal multiple access (OMA) [2], [3]. It is well known that the underlying principles of NOMA such as the superposition coding and SIC were proposed by Cover for broadcast channels (BCs) [5], [6]. Originally designed for decoding multiuser signal in multiple access channels (MACs) [7], SIC is now regarded as a general receiver structure for the uplink NOMA [2], [3]. Due to inter-user interference, NOMA applications face the challenges of decreased throughput, poor fairness, complexity issue and SIC processing delay. To meet new requirements of 5G and beyond 5G networks on quality of service (QoS), quality of experience (QoE), and other system performance metrics, diverse NOMA topics have been investigated (see [2], [3], and references therein).

A. Technical Literature Review

For downlink NOMA, it has been shown that two users with more distinctive channel gains should be paired to increase the sum rate [8]. Practically, grouping a limited number of users to share the same resource block can alleviate inter-user interference, whereas the user fairness is still critical due to asymmetric channel qualities [9]. Based on either instantaneous or statistical channel state information (CSI), a max-min fairness targeted power allocation scheme was proposed in [10]. Several grouping and scheduling schemes were proposed to maximize the sum rate taking into account the user fairness [11]–[14]. Moreover, the joint resource and power allocation schemes were proposed to achieve the allowed maximum sum rate from the perspective of fairness [15]–[17]. Taking into account the commonly adopted Jain's index, a new fairness metric was introduced for NOMA users by measuring the deviations between the achieved data rates and fair data rates [18].

In uplink NOMA systems, signals from multiple users are naturally superimposed at a base station (BS) and the channel disparity resulted by different path-losses is critical for increasing the sum rate and achieving the user fairness. It has been shown that a user can be always in outage under improper targeted data rate in uplink NOMA [19]. Based on instantaneous CSI, a dynamic power allocation scheme was proposed to ensure that a larger transmission rate was achieved over that of conventional OMA [20]. To guarantee user fairness, an outage-constrained min-max power allocation scheme was proposed in [21] and a game theory-based power allocation scheme was proposed in [22]. In [23], a QoE-oriented power allocation scheme was proposed to achieve the multiuser diversity. Various SIC receivers with dynamic decoding orders were proposed to improve the decoding performance [24]–[26].

H. Liu is with the School of Information Science and Electrical Engineering, Shandong Jiaotong University, Jinan 250357, China (e-mail: liuhongwu@sdjtu.edu.cn).

T. A. Tsiftsis is with the School of Intelligent Systems Science and Engineering, Jinan University, Zhuhai 519070, China (e-mail: theo_tsiftsis@jnu.edu.cn).

K. J. Kim is with Mitsubishi Electric Research Laboratories, Cambridge, MA 02139 USA (e-mail: kkim@merl.com).

K. S. Kwak is with the Department of Information and Communication Engineering, Inha University, Incheon 22212, South Korea (e-mail: kskwak@inha.ac.kr).

H. V. Poor is with the Department of Electrical Engineering, Princeton University, Princeton, NJ 08544 USA (e-mail: poor@princeton.edu).

Parts of this paper were presented at the IEEE International Conference on Communications 2019 [1].

Highlighted by delivering messages of different types to multiple users, rate splitting (RS) techniques have gained a lot of attention recently [27]–[30]. For the two-user interference channels, it has been shown that RS can achieve the allowed largest capacity region [31]. For multi-cell networks, the maximum achievable rate has been significantly improved by applying RS [32]. Based on imperfect CSI at the transmitter (CSIT), the optimized common message precoder has been investigated for multiple input single output (MISO) channels [33]. Moreover, the optimized RS precoder has been studied under imperfect CSIT for multiuser MISO systems with massive transmit antennas deployments [34]. For non-orthogonal unicast and multicast channels, it has been shown that RS-aided multiple access techniques provided a bridge between NOMA and space-division multiple access (SDMA) [35]. In [36], RS was applied to enhance the physical layer security performance for NOMA-based full-duplex relay systems. In [37], RS was applied to maximize the weighted sum rate for a multiuser MISO system with wireless information and power transfer [37]. It should be noted that RS can achieve the capacity region of the MACs [38], [39], whereas most of the above RS schemes were investigated for the BCs. For uplink NOMA systems, the heuristic RS scheme was proposed to achieve the same sum rate as that of the belief propagation strategy [40], while the exhaustive searching based RS scheme was proposed to maximize the minimum data rate [41].

B. Motivation

Being regarded as a practical way for achieving the capacity region of the MACs [38], [39], RS and its applications for delay-limited transmissions are still at infantry stages, e.g., the RS applications in uplink NOMA [40]–[42]. It has been shown that the RS schemes with the heuristic and exhaustive searching strategies involved huge computational complexity [40], [41]. Without considering the channel gain disparity and user fairness, one way for reducing user pairing complexity is to pair only two users in each group [42]. In delay-limited transmissions, the targeted data rates and transmit power allocation are crucial to maintain user fairness and improve outage performance [1]. Moreover, several practical restrictions exist in the uplink NOMA, including high peak-to-average power ratio (PAPR) [43] and imperfect synchronization [44], [45]. A promising waveform solution for avoiding the high PAPR and strict synchronization requirements is cyclic prefixed single carrier (CP-SC) transmission, which is robust to not only phase noise but also carrier frequency offset in frequency-selective fading channels [46], [47]. Employing either null CP or block-wise data CP, CP-SC was applied for massive multiple-input multiple-output (MIMO) communications and millimeter wave communications [48], [49]. Nevertheless, CP-SC and CP-SC-based RS have not yet been applied for the uplink NOMA.

In this paper, RS is applied as an effective way to achieve user fairness and improve outage performance for an uplink NOMA system in delay-limited transmissions. Based on achievable rate region analysis, the transmit power allocation, targeted data rates allocation, and the SIC decoding order are investigated. Meanwhile, CP-SC is adopted as a practical transmission waveform for uplink NOMA taking into account frequency-selective fading channels.

C. Our Contributions

The main contributions of this paper are summarized as follows:

- CP-SC transmission is applied for uplink NOMA over frequency selective fading channels. At the BS, the superimposed multi-user signals are detected using frequency-domain equalization (FDE) and the impact of synchronization errors on SIC processing can be effectively eliminated using phase compensation.
- Fixed RS (FRS) and cognitive RS (CRS) schemes are proposed to enhance the user fairness and outage performance for uplink NOMA in delay-limited transmissions. Fixed power allocation and cognitive power allocation are proposed for the FRS and CRS schemes, respectively. Based on the achievable rate region analysis, the benefits of applying RS for improving user fairness and outage performance are revealed. A modified Jain's index is proposed to measure the user fairness for the considered delay-limited transmissions.
- Closed-form expressions are derived for the outage probabilities of both users when the FRS and CRS schemes are deployed, respectively. Asymptotic outage probability expressions are derived for the FRS and CRS schemes, respectively. The impacts of the targeted data rates allocation and transmit power allocation on the outage performance of the considered system are revealed. The enhanced user fairness and superior outage performance achieved by the proposed FRS and CRS schemes are corroborated by Monte Carlo simulation results.

The remainder of this paper is organized as follows: Section II presents the system model of the uplink NOMA; In Section III, the FRS schemes are proposed to realize RS at the near and far users, respectively, and the user fairness and outage performance analysis are presented; In Section IV, the CRS schemes are proposed to realize RS at the near and far users, respectively; In Section V, simulation results are presented for corroborating the superior outage performance of the FRS and CRS schemes and Section VI summarizes this work.

Notation: Matrices and vectors are denoted by upper- and lower-case boldface letters, respectively. $x \sim \mathcal{CN}(\mu, \sigma^2)$ denotes that x follows the complex Gaussian distribution with mean μ and variance σ^2. $f_\varphi(\cdot)$ and $F_\varphi(\cdot)$ denote the probability density function (PDF) and cumulative distribution function (CDF) of the random variable (RV) φ, respectively. $\boldsymbol{I}_N$ is the $N \times N$ identity matrix.

II. System Model

We assume a conventional uplink NOMA scenario, where a near user U_1 and a far user U_2 are paired to share the same time-frequency resource block. For frequency-selective fading channels, we use $\boldsymbol{h}_i$ to denote the small-scale fading channel from U_i to the BS with $i = 1$ and 2 and assume $\boldsymbol{h}_i \sim \mathcal{CN}(0, \boldsymbol{I}_{N_i})$, where N_i is the length of $\boldsymbol{h}_i$ [50], [51]. In addition, the path-loss associated with $\boldsymbol{h}_i$ is denoted

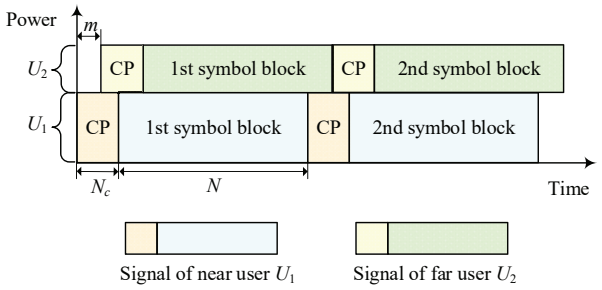

Fig. 1. Illustration of the arrived signals at the BS with a time offset.

by $\mathcal{L}_i$. The transmitted symbol block of U_i is denoted by $\boldsymbol{x}_i \sim \mathcal{CN}(\boldsymbol{0}, \boldsymbol{I}_N)$, where N is the number of the symbols in each symbol block. To prevent inter-block symbol interference (IBSI), the CP comprising of N_c last symbol of $\boldsymbol{x}_i$ is appended to the front of $\boldsymbol{x}_i$ with N_c satisfying $N_c > \max(N_1, N_2)$.

In uplink NOMA systems, the signals transmitted by the users are naturally superimposed at the BS in the power-domain. Due to synchronization timing errors and coordination time errors [44], [45], perfect synchronization in the uplink NOMA can hardly be achieved. Moreover, radio propagations from the randomly located users to the BS have unequal propagation times. Consequently, the signals transmitted from different users arrive at the BS having a high probability to be misaligned for SIC. Without loss of generality, we assume that the far user's signal always arrives at the BS after the arrival of the near user's signal with a relative time offset m ($m < N_c$), as depicted in Fig. 1. At the BS, the near user's signal is first detected by treating the far user's signal as noise. Then, SIC is performed for detecting the far user's signal. Before detecting the near user's signal, the CP-related components are removed from the received signal with the remained signal given by [50], [51]

$$\boldsymbol{y} = \sqrt{P_1\mathcal{L}_1}\boldsymbol{H}_1\boldsymbol{x}_1 + \sqrt{P_2\mathcal{L}_2}\boldsymbol{\Pi}_m\boldsymbol{H}_2\boldsymbol{x}_2 + \boldsymbol{z}, \tag{1}$$

where P_i is the transmit power of U_i, $\boldsymbol{H}_i$ is the $N \times N$ right circulant matrix specified by $\boldsymbol{h}_i$, $\boldsymbol{\Pi}_m$ denotes the $N \times N$ orthogonal permutation matrix obtained by circularly shifting down $\boldsymbol{I}_N$ by m rows, and $\boldsymbol{z} \sim \mathcal{CN}(\boldsymbol{0}, \sigma^2\boldsymbol{I}_N)$ is the additive white Gaussian noise (AWGN) at the BS. With the received signal $\boldsymbol{y}$, FDE is applied for detecting the near user's signal. Denoting the $N \times N$ discrete Fourier transform (DFT) matrix by $\boldsymbol{F}$, whose (p, q)th entry is given by $\frac{1}{\sqrt{N}}e^{-j2\pi pq/N}$, the converted frequency-domain signal can be expressed as

$$\widetilde{\boldsymbol{y}} = \boldsymbol{F}\boldsymbol{y} = \sqrt{\bar{P}_1}\widetilde{\boldsymbol{H}}_1\boldsymbol{F}\boldsymbol{x}_1 + \sqrt{\bar{P}_2}\boldsymbol{Q}\widetilde{\boldsymbol{H}}_2\boldsymbol{F}\boldsymbol{x}_2 + \boldsymbol{F}\boldsymbol{z}, \tag{2}$$

where $\bar{P}_i \triangleq P_i\mathcal{L}_i$, $\widetilde{\boldsymbol{H}}_i = \mathrm{diag}\big\{\mathrm{DFT}(\boldsymbol{h}_i)\big\}$ is the channel frequency response matrix and $\boldsymbol{Q}$ is an $N \times N$ diagonal matrix with its (n, n)th entry given by $e^{j2\pi m(n-1)/N}$. Then, FDE is performed with the resulted estimate of $\boldsymbol{x}_1$ given by

$$\begin{aligned}\widehat{\boldsymbol{x}}_1 &= \boldsymbol{F}^H\widetilde{\boldsymbol{H}}_1^{-1}\widetilde{\boldsymbol{y}} \\ &= \sqrt{\bar{P}_1}\boldsymbol{x}_1 + \sqrt{\bar{P}_2}\boldsymbol{F}^H\widetilde{\boldsymbol{H}}_1^{-1}\boldsymbol{Q}\widetilde{\boldsymbol{H}}_2\boldsymbol{F}\boldsymbol{x}_2 + \boldsymbol{F}^H\widetilde{\boldsymbol{H}}_1^{-1}\boldsymbol{F}\boldsymbol{z}.\end{aligned} \tag{3}$$

Based on (2) and (3), the received signal-to-interference-plus-noise ratio (SINR) for detecting $\boldsymbol{x}_1$ can be derived as [50], [51]

$$\gamma_1 = \frac{\bar{P}_1||\boldsymbol{h}_1||^2}{\bar{P}_2||\boldsymbol{h}_2||^2 + \sigma^2} = \frac{\rho||\boldsymbol{h}_1||^2}{\varepsilon\rho||\boldsymbol{h}_2||^2 + 1}, \tag{4}$$

where $\rho = \bar{P}_1/\sigma^2$ is the equivalent SNR measured for U_1 and $\varepsilon = \frac{P_2\mathcal{L}_2}{P_1\mathcal{L}_1}$ is a constant reflecting the large-scale fading disparity between two users. After recovering $\boldsymbol{x}_1$ from $\hat{\boldsymbol{x}}_1$, the reconstructed frequency-domain signal is subtracted from (2) with its form given by

$$\widehat{\boldsymbol{y}} = \sqrt{\bar{P}_2}\boldsymbol{Q}\widetilde{\boldsymbol{H}}_2\boldsymbol{F}\boldsymbol{x}_2 + \boldsymbol{F}\boldsymbol{z}. \tag{5}$$

With the aid of the phase compensation $\boldsymbol{Q}^{-1}$ and FDE, the estimate of $\boldsymbol{x}_2$ is obtained as

$$\widehat{\boldsymbol{x}}_2 = \boldsymbol{F}^H\widetilde{\boldsymbol{H}}_2^{-1}\boldsymbol{Q}^{-1}\widehat{\boldsymbol{y}} = \sqrt{\bar{P}_2}\boldsymbol{x}_2 + \boldsymbol{F}^H\widetilde{\boldsymbol{H}}_2^{-1}\boldsymbol{Q}^{-1}\boldsymbol{F}\boldsymbol{z}. \tag{6}$$

Based on (6), the received SNR for detecting $\boldsymbol{x}_2$ can be derived as

$$\gamma_2 = \frac{\bar{P}_2||\boldsymbol{h}_2||^2}{\sigma^2} = \varepsilon\rho||\boldsymbol{h}_2||^2. \tag{7}$$

For U_1 and U_2, the achievable rates are given by $R_1^{\mathrm{NOMA}} = \log_2(1+\gamma_1)$ and $R_2^{\mathrm{NOMA}} = \log_2(1+\gamma_2)$, respectively. For U_i, we denote its targeted transmit rate by $\widehat{R}_i$. Then, the required SINR/SNR threshold for achieving $\widehat{R}_i$ can be expressed as $\widehat{\gamma}_i = 2^{\widehat{R}_i} - 1$. In the detection of $\boldsymbol{x}_1$, an outage event occurs when $\gamma_1 < \widehat{\gamma}_1$. In the detection of $\boldsymbol{x}_2$, the outage events include two cases: 1) $\gamma_1 < \widehat{\gamma}_1$; 2) $(\gamma_1 \geq \widehat{\gamma}_1) \cap (\gamma_2 < \widehat{\gamma}_2)$. Then, the analytical expressions for the outage probabilities of U_1 and U_2, $P_{\mathrm{out},1}$ and $P_{\mathrm{out},2}$, can be expressed as (11) and (12) of [1], respectively. It has also been shown that asymptotic outage probabilities U_1 and U_2 are the same [1]. Based on the derived outage probability expressions, the average throughputs of U_1 and U_2 can be expressed as $\bar{R}_1 = (1 - P_{\mathrm{out},1})\widehat{R}_1$ and $\bar{R}_2 = (1 - P_{\mathrm{out},2})\widehat{R}_2$, respectively.

III. FRS Scheme

For the MAC with two users, it has been shown that only a single user's signal needs to be split to achieve the capacity region [38], [39]. Motivated by this, we propose two FRS schemes, namely, the FRS-N and FRS-F schemes, which deploy RS at the near and far users, respectively, with the aim of enhancing the user fairness and outage performance.

A. FRS-N Scheme

In the FRS-N scheme, only $\boldsymbol{x}_1$ is split into two data streams $\boldsymbol{x}_{11}$ and $\boldsymbol{x}_{12}$, respectively, which correspond to two virtual users U_{11} and U_{12}, respectively. Then, the received frequency-domain signal at the BS can be written as

$$\begin{aligned}\widetilde{\boldsymbol{y}} =& \sqrt{\alpha\bar{P}_1}\widetilde{\boldsymbol{H}}_1\boldsymbol{F}\boldsymbol{x}_{11} + \sqrt{(1-\alpha)\bar{P}_1}\widetilde{\boldsymbol{H}}_1\boldsymbol{F}\boldsymbol{x}_{12} \\ &+ \sqrt{\bar{P}_2}\boldsymbol{Q}\widetilde{\boldsymbol{H}}_2\boldsymbol{F}\boldsymbol{x}_2 + \boldsymbol{F}\boldsymbol{z},\end{aligned} \tag{8}$$

where α is the power allocation factor. In addition, the targeted data rates for transmitting $\boldsymbol{x}_{11}$ and $\boldsymbol{x}_{12}$ are set by $\widehat{R}_{11} = \beta\widehat{R}_1$ and $\widehat{R}_{12} = (1-\beta)\widehat{R}_1$, respectively, where $0 < \beta < 1$ is the targeted data rate factor.

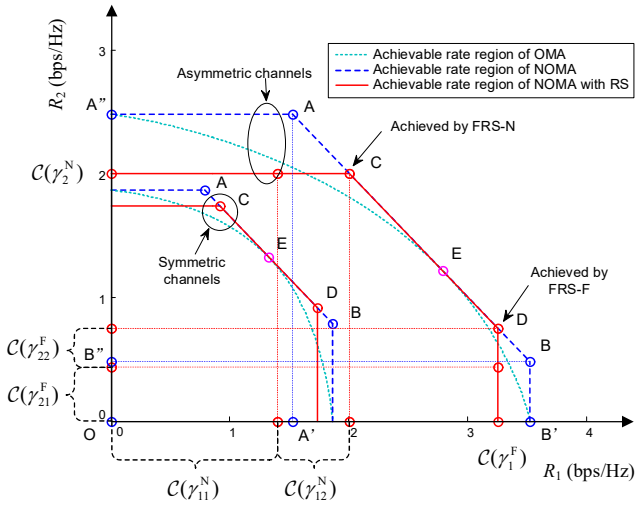

Fig. 2. The achievable rate regions of NOMA, NOMA with RS, and OMA with optimal DoF allocation for a single channel realization. For the curves of asymmetric channels, we have $\rho = 15$ dB, $\varepsilon = -4$ dB, $||\boldsymbol{h}_1||^2 = 0.333$, and $||\boldsymbol{h}_2||^2 = 0.364$. For the curves of symmetric channels, we have $\rho = 9$ dB, $\varepsilon = 0$ dB, and $||\boldsymbol{h}_1||^2 = ||\boldsymbol{h}_2||^2 = 0.333$. For NOMA with RS, we use a fixed value of $\alpha = 0.95$.

At the BS, SIC is applied for detecting $\boldsymbol{x}_{11}$, $\boldsymbol{x}_{12}$, and $\boldsymbol{x}_2$, respectively. By using α and $1-\alpha$ interchangeably in (8), all the possible decoding orders of SIC can be classified into three equivalent cases, i.e., 1) $\boldsymbol{x}_{11} \to \boldsymbol{x}_{12} \to \boldsymbol{x}_2$, 2) $\boldsymbol{x}_2 \to \boldsymbol{x}_{11} \to \boldsymbol{x}_{12}$, and 3) $\boldsymbol{x}_{11} \to \boldsymbol{x}_2 \to \boldsymbol{x}_{12}$. Irrespective of these decoding orders, the achievable rates obtained by the FRS-N scheme for U_1 and U_2 are given by $\mathcal{C}(\gamma_{11}^{\mathrm{N}}) + \mathcal{C}(\gamma_{12}^{\mathrm{N}})$ and $\mathcal{C}(\gamma_2^{\mathrm{N}})$, respectively, where $\mathcal{C}(\gamma) \triangleq \log_2(1+\gamma)$ denotes the achievable rate and γ_{11}^{N}, γ_{12}^{N}, and γ_2^{N} denote the received SINR/SNR for detecting $\boldsymbol{x}_{11}$, $\boldsymbol{x}_{12}$, and $\boldsymbol{x}_2$, respectively, which can be obtained following a similar procedure as those for (4) and (7) [50], [51]. To determine a suitable decoding order for the FRS-N scheme, an example of the achievable rate region comparison is presented in Fig. 2 for OMA, NOMA, and NOMA with RS schemes. As shown in Fig. 2, the corner points A and B are achieved by the conventional NOMA with SIC, while any rate pairs on the line segments between the corner points can be achieved via a time sharing or RS strategy [38], [39]. When the decoding order $\boldsymbol{x}_{11} \to \boldsymbol{x}_{12} \to \boldsymbol{x}_2$ is applied in the FRS-N scheme, it achieves the point A as that of the conventional NOMA with the decoding order $\boldsymbol{x}_1 \to \boldsymbol{x}_2$ due to $\mathcal{C}(\gamma_{11}^{\mathrm{N}}) + \mathcal{C}(\gamma_{11}^{\mathrm{N}}) = \mathcal{C}(\gamma_1)$ and $\mathcal{C}(\gamma_2^{\mathrm{N}}) = \mathcal{C}(\gamma_2)$. Also, it can be shown that the FRS-N scheme with the decoding order $\boldsymbol{x}_2 \to \boldsymbol{x}_{11} \to \boldsymbol{x}_{12}$ can only achieve the point B as that of the conventional NOMA with the decoding order $\boldsymbol{x}_2 \to \boldsymbol{x}_1$. On the other hand, when the decoding order $\boldsymbol{x}_{11} \to \boldsymbol{x}_2 \to \boldsymbol{x}_{12}$ is applied, the FRS-N scheme can achieve any points between A and B on the achievable rate region boundary. Therefore, the decoding order $\boldsymbol{x}_{11} \to \boldsymbol{x}_2 \to \boldsymbol{x}_{12}$ is applied in the FRS-N scheme.

With the aid of FDE, the estimate of $\boldsymbol{x}_{11}$ is given by

$$\begin{aligned}\widehat{\boldsymbol{x}}_{11} =& \boldsymbol{F}^H \widetilde{\boldsymbol{H}}_1^{-1} \widetilde{\boldsymbol{y}} \\ =& \sqrt{\alpha \bar{P}_1}\boldsymbol{x}_{11} + \sqrt{(1-\alpha)\bar{P}_1}\boldsymbol{x}_{12} \\ &+ \sqrt{\bar{P}_2}\boldsymbol{F}^H \widetilde{\boldsymbol{H}}_1^{-1}\boldsymbol{Q}\widetilde{\boldsymbol{H}}_2\boldsymbol{F}\boldsymbol{x}_2 + \boldsymbol{F}^H \widetilde{\boldsymbol{H}}_1^{-1}\boldsymbol{F}\boldsymbol{z}.\end{aligned} \tag{9}$$

Based on (9), the received SINR for detecting $\boldsymbol{x}_{11}$ can be derived as

$$\gamma_{11}^{\mathrm{N}} = \frac{\alpha\rho||\boldsymbol{h}_1||^2}{(1-\alpha)\rho||\boldsymbol{h}_1||^2 + \varepsilon\rho||\boldsymbol{h}_2||^2 + 1}. \tag{10}$$

After recovering $\boldsymbol{x}_{11}$ and subtracting its reconstructed version from (8), the remainded signal for detecting $\boldsymbol{x}_2$ and $\boldsymbol{x}_{12}$ can be generated as

$$\widehat{\boldsymbol{y}} = \sqrt{\bar{P}_2}\boldsymbol{Q}\widetilde{\boldsymbol{H}}_2\boldsymbol{F}\boldsymbol{x}_2 + \sqrt{(1-\alpha)\bar{P}_1}\widetilde{\boldsymbol{H}}_1\boldsymbol{F}\boldsymbol{x}_{12} + \boldsymbol{F}\boldsymbol{z}. \tag{11}$$

Based on (11), applying the phase compensation $\boldsymbol{Q}^{-1}$, FDE, and inverse DFT, the estimate of $\boldsymbol{x}_2$ is given by

$$\begin{aligned}\widehat{\boldsymbol{x}}_2 =& \sqrt{\bar{P}_2}\boldsymbol{x}_2 + \sqrt{(1-\alpha)\bar{P}_1}\boldsymbol{F}^H \widetilde{\boldsymbol{H}}_2^{-1}\boldsymbol{Q}^{-1}\widetilde{\boldsymbol{H}}_1\boldsymbol{F}\boldsymbol{x}_{12} \\ &+ \boldsymbol{F}^H \widetilde{\boldsymbol{H}}_2^{-1}\boldsymbol{Q}^{-1}\boldsymbol{F}\boldsymbol{z}.\end{aligned} \tag{12}$$

At the final stage of SIC, the estimate of $\boldsymbol{x}_{12}$ can be expressed as

$$\widehat{\boldsymbol{x}}_{12} = \sqrt{(1-\alpha)\bar{P}_1}\boldsymbol{x}_{12} + \boldsymbol{F}^H \widetilde{\boldsymbol{H}}_1^{-1}\boldsymbol{F}\boldsymbol{z}. \tag{13}$$

Based on (12) and (13), the received SINR and SNR for detecting $\boldsymbol{x}_2$ and $\boldsymbol{x}_{12}$ can be derived as

$$\gamma_2^{\mathrm{N}} = \frac{\varepsilon\rho||\boldsymbol{h}_2||^2}{(1-\alpha)\rho||\boldsymbol{h}_1||^2 + 1} \tag{14}$$

and

$$\gamma_{12}^{\mathrm{N}} = (1-\alpha)\rho||\boldsymbol{h}_1||^2, \tag{15}$$

respectively. Considering the symmetry between U_1 and U_2 in the uplink NOMA, the FRS-F scheme is also briefly described in the next subsection.

B. FRS-F Scheme

In the FRS-F scheme, $\boldsymbol{x}_2$ is split into two sub-symbol blocks $\boldsymbol{x}_{21}$ and $\boldsymbol{x}_{22}$, respectively. Then, the received frequency-domain signal at the BS can be written as

$$\begin{aligned}\widetilde{\boldsymbol{y}} =& \sqrt{\bar{P}_1}\widetilde{\boldsymbol{H}}_1\boldsymbol{F}\boldsymbol{x}_1 + \sqrt{\alpha\bar{P}_2}\boldsymbol{Q}\widetilde{\boldsymbol{H}}_2\boldsymbol{F}\boldsymbol{x}_{21} \\ &+ \sqrt{(1-\alpha)\bar{P}_2}\boldsymbol{Q}\widetilde{\boldsymbol{H}}_2\boldsymbol{F}\boldsymbol{x}_{22} + \boldsymbol{F}\boldsymbol{z}.\end{aligned} \tag{16}$$

In the FRS-F scheme, the targeted data rates for transmitting $\boldsymbol{x}_{21}$ and $\boldsymbol{x}_{22}$ are set by $\widehat{R}_{21} = \beta\widehat{R}_2$ and $\widehat{R}_{22} = (1-\beta)\widehat{R}_2$, respectively. Similar to the decoding order chosen for the FRS-N scheme, the decoding order $\boldsymbol{x}_{21} \to \boldsymbol{x}_1 \to \boldsymbol{x}_{22}$ is applied in the FRS-F scheme. Accordingly, the received SINR/SNR for detecting $\boldsymbol{x}_{21}$, $\boldsymbol{x}_1$, and $\boldsymbol{x}_{22}$ can be derived as

$$\gamma_{21}^{\mathrm{F}} = \frac{\alpha\varepsilon\rho||\boldsymbol{h}_2||^2}{\rho||\boldsymbol{h}_1||^2 + (1-\alpha)\varepsilon\rho||\boldsymbol{h}_2||^2 + 1}, \tag{17}$$

$$\gamma_1^{\mathrm{F}} = \frac{\rho||\boldsymbol{h}_1||^2}{(1-\alpha)\varepsilon\rho||\boldsymbol{h}_2||^2 + 1}, \tag{18}$$

and

$$\gamma_{22}^{\mathrm{F}} = (1-\alpha)\varepsilon\rho||\boldsymbol{h}_2||^2, \tag{19}$$

respectively. Then, the achievable rates obtained by the FRS-F scheme with the decoding order $\boldsymbol{x}_{21} \to \boldsymbol{x}_1 \to \boldsymbol{x}_{22}$ for U_1 and U_2 can be expressed as $R_1^{\mathrm{FRS-F}} = \log_2(1+\gamma_1^{\mathrm{F}})$ and $R_2^{\mathrm{FRS-F}} = \log_2(1+\gamma_{21}^{\mathrm{F}}) + \log_2(1+\gamma_{22}^{\mathrm{F}})$, respectively.

C. Achievable Rate Region and Fairness Analysis

With the optimal degrees of freedom (DoF) allocation, OMA can achieve the same sum rate as that of NOMA [39], [52]. As shown in Fig. 2, the optimal point E that maximizes the sum rate for OMA lies on the achievable rate region boundary of NOMA. Since the achievable rate region of OMA is a subset of that of NOMA, NOMA always outperforms OMA on the user fairness and spectral efficiency.

Corresponding to the corner point A achieved by NOMA over asymmetric channels in Fig. 2, any targeted rate pair $\left(\widehat{R}_1, \widehat{R}_2\right)$ lies in the rectangle with the vertices {O, A', A, A"} can be satisfied by applying NOMA, i.e., the rectangle with the vertices {O, A', A, A"} is the non-outage zone achieved by NOMA with the decoding order $\boldsymbol{x}_1 \rightarrow \boldsymbol{x}_2$. Similarly, the rectangle with the vertices {O, B', B, B"} is the non-outage zone achieved by NOMA with the decoding order $\boldsymbol{x}_2 \rightarrow \boldsymbol{x}_1$. Compared to the non-outage zones determined by the corner points A and B, respectively, the non-outage zone achieved by the FRS-N scheme via adjusting α is the zone with the vertices {O, B', B, A, A"}, which includes the rectangles {O, A', A, A"} and {O, B', B, B"} as the subsets, respectively. Consequently, the FRS-N scheme can achieve a better outage performance than those achieved by the NOMA schemes corresponding to the corner points A and B.

In the sense of Jain's index for measuring the user fairness, it has been shown that the corner points achieved by NOMA with SIC is fairer than OMA with the optimal DoF allocation when the channel disparity satisfies (11) of [9]. As per the asymmetric channels in Fig. 2, the corner point A achieved by NOMA is fairer than the optimal point E achieved by OMA. Nevertheless, we can apply the FRS-N scheme with the decoding order $\boldsymbol{x}_{11} \rightarrow \boldsymbol{x}_2 \rightarrow \boldsymbol{x}_{12}$ to achieve the corner point C, which is fairer than the point A. For the symmetric channels, even the optimal point E achieved by OMA is fairer than the corner points A and B achieved by NOMA, we can adjust α for the FRS scheme such that the points C and D move to the position of the point E. Besides, the points C and D can be coincident with the points A and B, respectively, by setting $\alpha = 1$. Thus, the FRS scheme always outperforms NOMA with SIC on the user fairness.

Unfortunately, the commonly adopted Jain's index is defined in terms of the achievable rates per channel use, while each user in the delay-limited transmission mode transmits at a fixed transmit rate corresponding to its QoS requirement. Considering that the fairness in delay-limited transmissions is affected by not only the users' QoS requirements, but also the average throughputs, we propose a modified Jain's index in the form of

$$J \triangleq \frac{\left(\sum_{k=1}^{K} \bar{R}_k\right)^2}{K\sum_{k=1}^{K} \widehat{R}_k^2} = \frac{\left(\sum_{k=1}^{K}(1-P_{\mathrm{out},k})\widehat{R}_k\right)^2}{K\sum_{k=1}^{K} \widehat{R}_k^2}, \quad (20)$$

where K is the number of total users in the considered system. According to (20), a scheme with a higher J is fairer and the allowed maximum value $J = 1$ is achieved only when all users have the same targeted transmit rate and experience non-outage events during the whole transmission periods. Moreover, $J < 1$ is strictly satisfied either $P_{\mathrm{out},k} > 0$ or $\widehat{R}_k \neq \widehat{R}_\ell$, $\forall k \neq \ell$. To eliminate the impact of different QoS requirements on the modified Jain's index, we can further express it in a normalized way as

$$J \triangleq \frac{1}{Q}\frac{\left(\sum_{k=1}^{K} \bar{R}_k\right)^2}{K\sum_{k=1}^{K} \widehat{R}_k^2} = \frac{\left(\sum_{k=1}^{K}(1-P_{\mathrm{out},k})\widehat{R}_k\right)^2}{\left(\sum_{k=1}^{K} \widehat{R}_k\right)^2}, \quad (21)$$

where $Q = \left(\sum_{k=1}^{K} \widehat{R}_k\right)^2 / \left(K\sum_{k=1}^{K} \widehat{R}_k^2\right)$ is the normalization factor. Consequently, when all users experience $P_{\mathrm{out},k} = 0$, $\forall k$, the modified Jain's index arrives $J = 1$ and the QoS-required fairness is achieved.

For the considered two-user case, the modified Jain's index can be expressed as

$$J = \frac{\left((1-P_{\mathrm{out},1})\widehat{R}_1 + (1-P_{\mathrm{out},2})\widehat{R}_2\right)^2}{\left(\widehat{R}_1 + \widehat{R}_2\right)^2}. \quad (22)$$

By given QoS requirements $\widehat{R}_1$ and $\widehat{R}_2$, an increasing outage probability $P_{\mathrm{out},1}$ (or $P_{\mathrm{out},2}$) always results in a decreasing modified Jain's index, which corresponds to a worse fairness, and vice verse. For the special case of $\widehat{R}_1 = \widehat{R}_2$, the modified Jain's index can be simplified as

$$J = \frac{(2 - P_{\mathrm{out},1} - P_{\mathrm{out},2})^2}{4} \quad (23)$$

and the ideal fairness $J = 1$ is achieved when $P_{\mathrm{out},1} = P_{\mathrm{out},2} = 0$. Since the FRS scheme achieves a better outage performance than NOMA due to the enlarged non-outage zone, the fairness obtained by the FRS scheme can be also enhanced over that of NOMA according to the modified Jain's index.

D. Outage Performance Analysis

In this section, the outage probabilities of U_1 and U_2 achieved by the FRS-N and FRS-F schemes are analyzed, respectively. For the virtual users U_{11} and U_{12} $\left(U_{21}$ and $U_{22}\right)$, the required SINR/SNR threshold for achieving $\widehat{R}_j$ can be expressed as $\widehat{\gamma}_j = 2^{\widehat{R}_j} - 1$ with $j \in \{11, 12, 21, 22\}$.

According to Fig. 2, any targeted rate pair $(\widehat{R}_1, \widehat{R}_2)$ lies out of the rectangular, whose left-down and right-up corners are the origin and point C, respectively, corresponds to an outage event. Therefore, the non-outage zone achieved by the FRS-N scheme for a channel realization is strictly restricted in this rectangular. However, even if $(\widehat{R}_1, \widehat{R}_2)$ lies in this rectangular, an outage event may still happen. For example, if either $\mathcal{C}(\gamma_{11}^{\mathrm{N}}) < \widehat{R}_{11}$, $\mathcal{C}(\gamma_2^{\mathrm{N}}) < \widehat{R}_2$, or $\mathcal{C}(\gamma_{12}^{\mathrm{N}}) < \widehat{R}_{12}$ happens, an outage event occurs for U_1. Accordingly, the outage events of U_1 can be classified into three cases: 1) $\mathcal{C}(\gamma_{11}^{\mathrm{N}}) < \widehat{R}_{11}$; 2) $(\mathcal{C}(\gamma_{11}^{\mathrm{N}}) \geq \widehat{R}_{11}) \cap (\mathcal{C}(\gamma_2^{\mathrm{N}}) < \widehat{R}_2)$; and 3) $(\mathcal{C}(\gamma_{11}^{\mathrm{N}}) \geq \widehat{R}_{11}) \cap (\mathcal{C}(\gamma_2^{\mathrm{N}}) \geq \widehat{R}_2) \cap (\mathcal{C}(\gamma_{12}^{\mathrm{N}}) < \widehat{R}_{21})$. Then, the outage probability of U_1 can be expressed as

$$\begin{aligned} P_{\mathrm{out},1} = {} & \Pr\left\{\gamma_{11}^{\mathrm{N}} < \widehat{\gamma}_{11}\right\} + \Pr\left\{(\gamma_{11}^{\mathrm{N}} \geq \widehat{\gamma}_{11}) \cap (\gamma_2^{\mathrm{N}} < \widehat{\gamma}_2)\right\} \\ & + \Pr\left\{(\gamma_{11}^{\mathrm{N}} \geq \widehat{\gamma}_{11}) \cap (\gamma_2^{\mathrm{N}} \geq \widehat{\gamma}_2) \cap (\gamma_{12}^{\mathrm{N}} < \widehat{\gamma}_{21})\right\}. \quad (24) \end{aligned}$$

As such, the outage probability of U_2 achieved by the FRS-N scheme can be written as

$$P_{\mathrm{out},2} = \Pr\left\{\gamma_{11}^{\mathrm{N}} < \widehat{\gamma}_{11}\right\} + \Pr\{(\gamma_{11}^{\mathrm{N}} \geq \widehat{\gamma}_{11}) \cap (\gamma_2^{\mathrm{N}} < \widehat{\gamma}_2)\}. \quad (25)$$

Theorem 1. *For the FRS-N scheme, the outage probabilities of U_1 and U_2 are given by $P_{\text{out},1} = 1 - I_1 + I_2$ and $P_{\text{out},2} = 1 - I_3 + I_4$, respectively, where*

$$I_1 \triangleq \frac{e^{-\frac{\widehat{\gamma}_2}{\varepsilon\rho}}}{\Gamma(N_1)} \sum_{n=0}^{N_2-1} \sum_{k=0}^{n} \frac{(1-\alpha)^k \rho^k}{n!} \left(\frac{\widehat{\gamma}_2}{\varepsilon\rho}\right)^n \binom{n}{k} \times \left(1+\tfrac{\widehat{\gamma}_2(1-\alpha)}{\varepsilon}\right)^{-N_1-k} \Gamma\left(N_1+k, \tfrac{\tau}{\rho}\left(1+\tfrac{\widehat{\gamma}_2(1-\alpha)}{\varepsilon}\right)\right), \quad (26)$$

$$I_2 \triangleq \frac{e^{-\frac{1}{\varepsilon\rho}}}{\Gamma(N_1)} \sum_{n=0}^{N_2-1} \sum_{k=0}^{n} \frac{(-1)^{n-k}}{\varepsilon^n \tau_2^k n!} \binom{n}{k} \left(1+\tfrac{1}{\varepsilon\tau_2}\right)^{-N_1-k} \times \Gamma\left(N_1+k, \tfrac{\tau}{\rho}\left(1+\tfrac{1}{\varepsilon\tau_2}\right)\right), \quad (27)$$

$$I_3 \triangleq \frac{e^{-\frac{\widehat{\gamma}_2}{\varepsilon\rho}}}{\Gamma(N_1)} \sum_{n=0}^{N_2-1} \sum_{k=0}^{n} \frac{(1-\alpha)^k \rho^k}{n!} \left(\frac{\widehat{\gamma}_2}{\varepsilon\rho}\right)^n \binom{n}{k} \times \left(1+\tfrac{\widehat{\gamma}_2(1-\alpha)}{\varepsilon}\right)^{-N_1-k} \Gamma\left(N_1+k, \tfrac{\tau_2}{\rho}\left(1+\tfrac{\widehat{\gamma}_2(1-\alpha)}{\varepsilon}\right)\right), \quad (28)$$

and

$$I_4 \triangleq \frac{e^{-\frac{1}{\varepsilon\rho}}}{\Gamma(N_1)} \sum_{n=0}^{N_2-1} \sum_{k=0}^{n} \frac{(-1)^{n-k}}{\varepsilon^n \tau_2^k n!} \binom{n}{k} \left(1+\tfrac{1}{\varepsilon\tau_2}\right)^{-N_1-k} \times \Gamma\left(N_1+k, \tfrac{\tau_2}{\rho}\left(1+\tfrac{1}{\varepsilon\tau_2}\right)\right) \quad (29)$$

with $\tau \triangleq \max\{\tau_1, \tau_2, \tau_3\}$, $\tau_1 \triangleq \frac{\widehat{\gamma}_{12}}{1-\alpha}$, $\tau_2 \triangleq \frac{\widehat{\gamma}_{11}}{\alpha-(1-\alpha)\widehat{\gamma}_{11}}$, and $\tau_3 \triangleq \frac{(1+\widehat{\gamma}_2)\widehat{\gamma}_{11}}{\alpha-(1-\alpha)(1+\widehat{\gamma}_2)\widehat{\gamma}_{11}}$.

Proof: See Appendix A. ∎

It is worthy pointing out that the expressions in Theorem 1 exist only when $\alpha > \frac{\widehat{\gamma}_{11}}{1+\widehat{\gamma}_{11}}$, whereas $P_{\text{out},1} = P_{\text{out},2} = 1$ when $\alpha \leq \frac{\widehat{\gamma}_{11}}{1+\widehat{\gamma}_{11}}$. The results in Theorem 1 characterize the outage probabilities of U_1 and U_2 in terms of the transmit SNR, power allocation factor, targeted data rates, and CSI statistics, which can be easily evaluated by computer computation. However, the effects of the system parameters on the outage performance cannot be explicitly extracted from $P_{\text{out},1}$ and $P_{\text{out},2}$ due to their complicated forms. In the following, asymptotic outage probability and corresponding system parameters choosing are presented.

Proposition 1. *As $\rho \to \infty$, asymptotic outage probabilities of U_1 and U_2 achieved by the FRS-N scheme are the same, which is given by $P_{\text{out}}^{\infty} = 1 - I_5 + I_6$, where*

$$I_5 \triangleq \frac{1}{\Gamma(N_1)} \sum_{n=0}^{N_2-1} \frac{1}{n!} \left(\tfrac{(1-\alpha)\widehat{\gamma}_2}{\varepsilon}\right)^n \left(1+\tfrac{(1-\alpha)\widehat{\gamma}_2}{\varepsilon}\right)^{-N_1-n} \times \Gamma(N_1+n) \quad (30)$$

and

$$I_6 \triangleq \frac{1}{\Gamma(N_1)} \sum_{n=0}^{N_2-1} \frac{(\varepsilon\tau_2)^{-n}}{n!} \left(1+\tfrac{1}{\varepsilon\tau_2}\right)^{-N_1-n} \Gamma(N_1+n). \quad (31)$$

Proof: As $\rho \to \infty$, both $P_{\text{out},1}$ and $P_{\text{out},2}$ approach $P_{\text{out}}^{\infty} = 1 - \Pr\left\{(\gamma_{11}^{\text{N}} \geq \widehat{\gamma}_{11}) \cap (\gamma_2^{\text{N}} \geq \widehat{\gamma}_2)\right\}$. Using the high SNR approximation $\gamma_{11}^{\text{N}} \approx \frac{\alpha g_1}{(1-\alpha)g_1+\varepsilon g_2}$ and $\gamma_2^{\text{N}} \approx \frac{\varepsilon g_2}{(1-\alpha)g_1}$, we have $P_{\text{out}}^{\infty} = 1 - \Pr\left\{\frac{\varepsilon\widehat{\gamma}_{11} g_2}{\alpha-(1-\alpha)\widehat{\gamma}_{11}} \leq g_1 \leq \frac{\varepsilon g_2}{(1-\alpha)\widehat{\gamma}_2}\right\}$, which can be derived as $P_{\text{out}}^{\infty} = 1 - I_5 + I_6$ with I_5 and I_6 given by (30) and (31), respectively. ∎

The results in Proposition 1 show that the outage probabilities of U_1 and U_2 encounter the same floor in the high SNR region, which is resulted by the limited detecting performance for $\boldsymbol{x}_{11}$ and $\boldsymbol{x}_2$ in SIC. Moreover, the above expressions are still too complicated for extracting the optimal system parameters. For simplicity, we set $N_2 = 1$ for P_{out}^{∞}, i.e., flat fading channels. Then, it can be shown that P_{out}^{∞} decreases monotonically with increasing α and increases monotonically with increasing $\widehat{R}_{11}$ (or β). Thus, to achieve a small value for P_{out}^{∞}, a large α and a small β are suggested for the FRS-N scheme. Since γ_2^{N} increases monotonically with increasing α, $P_{\text{out},2}$ can be decreased with a large α. However, a large α results in the decreased γ_{12}^{N}, which indicates that a small α is also needed to guarantee a small value for $P_{\text{out},2}$ in the low and middle SNR regions. Therefore, a relative large α should be chosen for the FRS-N scheme considering the user fairness in the whole SNR region.

For the FRS-F scheme, the outage probabilities of U_1 and U_2 can be expressed as

$$P_{\text{out},1} = \Pr\left\{\gamma_{21}^{\text{F}} < \widehat{\gamma}_{21}\right\} + \Pr\left\{(\gamma_{21}^{\text{F}} \geq \widehat{\gamma}_{21}) \cap (\gamma_1^{\text{F}} < \widehat{\gamma}_1)\right\} \quad (32)$$

and

$$P_{\text{out},2} = \Pr\left\{\gamma_{21}^{\text{F}} < \widehat{\gamma}_{21}\right\} + \Pr\left\{(\gamma_{21}^{\text{F}} \geq \widehat{\gamma}_{21}) \cap (\gamma_1^{\text{F}} < \widehat{\gamma}_1)\right\} + \Pr\left\{(\gamma_{21}^{\text{F}} \geq \widehat{\gamma}_{21}) \cap (\gamma_1^{\text{F}} \geq \widehat{\gamma}_1) \cap (\gamma_{22}^{\text{F}} < \widehat{\gamma}_{22})\right\}, \quad (33)$$

respectively.

Theorem 2. *For the FRS-F scheme, the outage probabilities of U_1 and U_2 are given by $P_{\text{out},1} = 1 - \widetilde{I}_1 + \widetilde{I}_2$ and $P_{\text{out},2} = 1 - \widetilde{I}_3 + \widetilde{I}_4$, respectively, where*

$$\widetilde{I}_1 \triangleq \frac{e^{-\frac{\widehat{\gamma}_1}{\rho}}}{\Gamma(N_2)} \sum_{n=0}^{N_1-1} \sum_{k=0}^{n} \frac{\widehat{\gamma}_1^n \varepsilon^k (1-\alpha)^k}{\rho^{n-k} n!} \binom{n}{k} \times \left(1+\varepsilon\widehat{\gamma}_1(1-\alpha)\right)^{-N_2-k} \times \Gamma\left(N_2+k, \tfrac{\widetilde{\tau}_3}{\rho}\left(1+\varepsilon\widehat{\gamma}_1(1-\alpha)\right)\right), \quad (34)$$

$$\widetilde{I}_2 \triangleq \frac{e^{\frac{1}{\rho}}}{\Gamma(N_2)} \sum_{n=0}^{N_1-1} \sum_{k=0}^{n} \frac{(-1)^{n-k}}{\rho^{n-k} \widetilde{\tau}_2^k n!} \binom{n}{k} \left(1+\tfrac{1}{\widetilde{\tau}_2}\right)^{-N_2-k} \times \Gamma\left(N_2+k, \tfrac{\widetilde{\tau}_3}{\rho}\left(1+\tfrac{1}{\widetilde{\tau}_2}\right)\right), \quad (35)$$

$$\widetilde{I}_3 \triangleq \frac{e^{-\frac{\widehat{\gamma}_1}{\rho}}}{\Gamma(N_2)} \sum_{n=0}^{N_1-1} \sum_{k=0}^{n} \frac{\widehat{\gamma}_1^n \varepsilon^k (1-\alpha)^k}{\rho^{n-k} n!} \binom{n}{k} \times \left(1+\varepsilon\widehat{\gamma}_1(1-\alpha)\right)^{-N_2-k} \times \Gamma\left(N_2+k, \tfrac{\widetilde{\tau}}{\rho}\left(1+\varepsilon\widehat{\gamma}_1(1-\alpha)\right)\right), \quad (36)$$

and

$$\widetilde{I}_4 \triangleq \frac{e^{\frac{1}{\rho}}}{\Gamma(N_2)} \sum_{n=0}^{N_1-1} \sum_{k=0}^{n} \frac{(-1)^{n-k}}{\rho^{n-k}\widetilde{\tau}_2^k n!} \binom{n}{k} \left(1+\tfrac{1}{\widetilde{\tau}_2}\right)^{-N_2-k} \times\Gamma\left(N_2+k, \tfrac{\widetilde{\tau}}{\rho}\left(1+\tfrac{1}{\widetilde{\tau}_2}\right)\right) \quad (37)$$

with $\widetilde{\tau} \triangleq \max\{\widetilde{\tau}_1, \widetilde{\tau}_2, \widetilde{\tau}_3\}$, $\widetilde{\tau}_1 \triangleq \frac{\widehat{\gamma}_{22}}{\varepsilon(1-\alpha)}$, $\widetilde{\tau}_2 \triangleq \frac{\widehat{\gamma}_{21}}{\varepsilon(\alpha-(1-\alpha)\widehat{\gamma}_{21})}$, *and* $\widetilde{\tau}_3 \triangleq \frac{(1+\widehat{\gamma}_1)\widehat{\gamma}_{21}}{\varepsilon(\alpha-(1-\alpha)(1+\widehat{\gamma}_1)\widehat{\gamma}_{21})}$.

Considering the symmetry between the FRS-F and FRS-N schemes, a proof for Theorem 2 can be derived in a similar way as that of Theorem 1, so that it is omitted here. Note that $P_{\text{out},1} = P_{\text{out},2} = 1$ when $\alpha \leq \frac{\widehat{\gamma}_{21}}{1+\widehat{\gamma}_{21}}$ and the expressions in Theorem 2 exist only when $\alpha > \frac{\widehat{\gamma}_{21}}{1+\widehat{\gamma}_{21}}$.

Proposition 2. *As $\rho \to \infty$, asymptotic outage probabilities of U_1 and U_2 achieved by the FRS-F scheme are the same, which is given by $P_{\text{out}}^{\infty} = 1 - \widetilde{I}_5 + \widetilde{I}_6$, where*

$$\widetilde{I}_5 \triangleq \frac{1}{\Gamma(N_2)} \sum_{n=0}^{N_1-1} \frac{(\varepsilon\widehat{\gamma}_1(1-\alpha))^n \Gamma(N_2+n)}{(1+\varepsilon\widehat{\gamma}_1(1-\alpha))^{N_2+n} n!} \quad (38)$$

and

$$\widetilde{I}_6 \triangleq \frac{1}{\Gamma(N_2)} \sum_{n=0}^{N_1-1} \frac{\widetilde{\tau}_2^{-n}\Gamma(N_1+n)}{(1+1/\widetilde{\tau}_2)^{N_2+n} n!}. \quad (39)$$

Proof: As $\rho \to \infty$, both $P_{\text{out},1}$ and $P_{\text{out},2}$ approach $P_{\text{out}}^{\infty} = 1 - \Pr\left\{(\gamma_{21}^{\text{F}} \geq \widehat{\gamma}_{21}) \cap (\gamma_1^{\text{F}} \geq \widehat{\gamma}_1)\right\}$. Using the high SNR approximation $\gamma_{21}^{\text{F}} \approx \frac{\alpha\varepsilon g_2}{g_1+(1-\alpha)\varepsilon g_2}$ and $\gamma_1^{\text{F}} \approx \frac{g_1}{(1-\alpha)\varepsilon g_2}$, we have $P_{\text{out}}^{\infty} = 1 - \Pr\{\varepsilon\widehat{\gamma}_1 g_2(1-\alpha) \leq g_1 \leq g_2/\widetilde{\tau}_2\}$, which can be derived as $P_{\text{out}}^{\infty} = 1 - \widetilde{I}_5 + \widetilde{I}_6$ with $\widetilde{I}_5$ and $\widetilde{I}_6$ given by (38) and (39), respectively. ∎

The results in Proposition 2 show that $P_{\text{out},1}$ and $P_{\text{out},2}$ approach the same floor in the high SNR region. Similarly to that of the FRS-N scheme, a large α and a small β are suggested to achieve a small P_{out}^{∞} for the FRS-F scheme. Also, only a relative large α should be chosen for the FRS-N scheme to guarantee the user fairness.

IV. CRS Scheme

It has been show that the NOMA users can be treated as the primary and secondary users in the sense of the underlay cognitive radio [53]. Motivated by this, we propose the CRS-N and CRS-F schemes for realizing RS at the near and far users, respectively. Different from the FRS schemes, the power allocation factors of the CRS schemes are dynamically determined based on the instantaneous channel gains, whereas the targeted data rates for the split data streams need to be preseted due to the considered delay-limited transmissions.

A. CRS-N Scheme

In the CRS-N scheme, RS is employed at the near user and $\boldsymbol{x}_1$ is split into $\boldsymbol{x}_{11}$ and $\boldsymbol{x}_{12}$, respectively. When the decoding order $\boldsymbol{x}_{11} \to \boldsymbol{x}_2 \to \boldsymbol{x}_{12}$ is applied, U_{11}, U_2, and U_{12} can be treated as the primary, secondary, and tertiary users, respectively. Obviously, an unsuccessful detection of $\boldsymbol{x}_{11}$ or $\boldsymbol{x}_2$ results in an incorrect detection of $\boldsymbol{x}_{12}$, which in turn results in an outage event for U_1. Also, an unsuccessful detection of $\boldsymbol{x}_{11}$ results in an outage event for U_2. Thus, the power allocation factor is designed to satisfy the quality of service (QoS) requirements of U_{11}, U_2, and U_{12} sequentially according to the decoding order $\boldsymbol{x}_{11} \to \boldsymbol{x}_2 \to \boldsymbol{x}_{12}$.

It can be shown that α satisfying the QoS requirement $\gamma_{11}^{\text{N}} \geq \widehat{\gamma}_{11}$ is characterized by

$$\alpha \in [\widehat{\alpha}_{_N}, 1], \quad \text{subject to } \widehat{\gamma}_{11} \leq \frac{g_1}{1+\varepsilon g_2}, \quad (40)$$

where

$$\widehat{\alpha}_{_N} = \frac{\widehat{\gamma}_{11}}{1+\widehat{\gamma}_{11}}\left(1+\frac{1}{g_1}+\frac{\varepsilon g_2}{g_1}\right) \quad (41)$$

is the minimum value of α satisfying $\gamma_{11}^{\text{N}} \geq \widehat{\gamma}_{11}$ and the constraint $\widehat{\gamma}_{11} \leq \frac{g_1}{1+\varepsilon g_2}$ is applied to restrict $0 < \widehat{\alpha} \leq 1$. For the QoS requirement $\gamma_2^{\text{N}} \geq \widehat{\gamma}_2$, the qualified α is characterized by

$$\alpha \in [\widetilde{\alpha}_{_N}, 1], \quad \text{subject to } \widehat{\gamma}_2 \leq \varepsilon g_2, \quad (42)$$

where

$$\widetilde{\alpha}_{_N} = \max\left(0, 1+\frac{1}{g_1}-\frac{\varepsilon g_2}{\widehat{\gamma}_2 g_1}\right) \quad (43)$$

is the minimum value of α satisfying $\gamma_2^{\text{N}} \geq \widehat{\gamma}_2$ and the constraint $\widehat{\gamma}_2 \leq \varepsilon g_2$ is applied to restrict $\widetilde{\alpha} \leq 1$. Then, the power allocation factor satisfying both $\gamma_{11}^{\text{N}} \geq \widehat{\gamma}_{11}$ and $\gamma_2^{\text{N}} \geq \widehat{\gamma}_2$ can be characterized by

$$\alpha \in \begin{cases} [\max(\widehat{\alpha}_{_N}, \widetilde{\alpha}_{_N}), 1], & \widehat{\gamma}_{11} \leq \frac{g_1}{1+\varepsilon g_2} \text{ and } \widehat{\gamma}_2 \leq \varepsilon g_2, \\ \text{does not exist}, & \text{otherwise.} \end{cases} \quad (44)$$

Since that γ_{12}^{N} decreases monotonically with increasing α, to make the probability $\Pr\{\gamma_{12}^{\text{N}} \geq \widehat{\gamma}_{12}\}$ as large as possible, the power allocation factor needs to be minimized besides the constraint (44). Thus, the cognitive power allocation factor is given by

$$\alpha = \begin{cases} \max(\widehat{\alpha}_{_N}, \widetilde{\alpha}_{_N}), & \widehat{\gamma}_{11} \leq \frac{g_1}{1+\varepsilon g_2} \text{ and } \widehat{\gamma}_2 \leq \varepsilon g_2, \\ \text{does not exist}, & \text{otherwise.} \end{cases} \quad (45)$$

When $\widehat{\gamma}_{11} \leq \frac{g_1}{1+\varepsilon g_2}$ and $\widehat{\gamma}_2 \leq \varepsilon g_2$ occur, it can be shown that both $\gamma_{11}^{\text{N}} \geq \widehat{\gamma}_{11}$ and $\gamma_2^{\text{N}} \geq \widehat{\gamma}_2$ are satisfied by using the above power allocation. Therefore, the outage probabilities of U_1 and U_2 can be expressed as

$$\begin{aligned} P_{\text{out},1} =& 1-\Pr\Big\{\big(\widehat{\gamma}_{11} \leq \tfrac{g_1}{1+\varepsilon g_2}\big) \cap \big(\widehat{\gamma}_2 \leq \varepsilon g_2\big) \cap \big(\widehat{\alpha}_{_N} \geq \widetilde{\alpha}_{_N}\big) \\ & \cap \big(\gamma_{12}^{\text{N}}(\widehat{\alpha}_{_N}) \geq \widehat{\gamma}_{12}\big)\Big\} - \Pr\Big\{\big(\widehat{\gamma}_{11} \leq \tfrac{g_1}{1+\varepsilon g_2}\big) \\ & \cap \big(\widehat{\gamma}_2 \leq \varepsilon g_2\big) \cap \big(\widehat{\alpha}_{_N} < \widetilde{\alpha}_{_N}\big) \cap \big(\gamma_{12}^{\text{N}}(\widetilde{\alpha}_{_N}) \geq \widehat{\gamma}_{12}\big)\Big\} \end{aligned} \quad (46)$$

and

$$P_{\text{out},2} = 1 - \Pr\Big\{\big(\widehat{\gamma}_{11} \leq \tfrac{g_1}{1+\varepsilon g_2}\big) \cap \big(\widehat{\gamma}_2^{\text{N}} \leq \varepsilon g_2\big)\Big\}, \quad (47)$$

respectively.

Theorem 3. *For the CRS-N scheme, the outage probabilities of U_1 and U_2 are given by*

$$P_{\text{out},1} = 1 - \frac{e^{-\frac{\widehat{\gamma}_{11}+\widehat{\gamma}_{12}+\widehat{\gamma}_{11}\widehat{\gamma}_{12}}{\rho}}}{\Gamma(N_2)} \sum_{n=0}^{N_1-1}\sum_{k=0}^{n} \frac{(\varepsilon\widehat{\gamma}_{11})^k}{n!}\binom{n}{k} \times\left(\frac{\widehat{\gamma}_{11}+\widehat{\gamma}_{12}+\widehat{\gamma}_{11}\widehat{\gamma}_{12}}{\rho}\right)^{n-k}\left(1+\varepsilon\widehat{\gamma}_{11}\right)^{-N_2-k} \times\Gamma\Big(N_2+k, \tfrac{\widehat{\gamma}_2(1+\widehat{\gamma}_{12})(1+\varepsilon\widehat{\gamma}_{11})}{\varepsilon\rho}\Big) \quad (48)$$

and

$$P_{\text{out},2} = 1 - \frac{e^{-\frac{\widehat{\gamma}_{11}}{\rho}}}{\Gamma(N_2)} \sum_{n=0}^{N_1-1}\sum_{k=0}^{n} \frac{\varepsilon^k\widehat{\gamma}_{11}^n}{\rho^{n-k}n!}\binom{n}{k} \times\left(1+\varepsilon\widehat{\gamma}_{11}\right)^{-N_2-k}\Gamma\Big(N_2+k, \tfrac{\widehat{\gamma}_2(1+\varepsilon\widehat{\gamma}_{11})}{\varepsilon\rho}\Big), \quad (49)$$

respectively.

Proof: See Appendix B. ∎

Proposition 3. *As $\rho \to \infty$, asymptotic outage probabilities of U_1 and U_2 achieved by the CRS-N scheme are the same, which is given by*

$$P_{\text{out}}^{\infty} = 1 - \frac{1}{\Gamma(N_2)} \sum_{n=0}^{N_1-1} \frac{(\varepsilon\widehat{\gamma}_{11})^n\Gamma(N_2+n)}{(1+\varepsilon\widehat{\gamma}_{11})^{N_2+n}n!} \quad (50)$$

Proof: As $\rho \to \infty$, we have an asymptotic expression $\widehat{\gamma}_{11} \leq \frac{g_1}{\varepsilon g_2}$ for $\widehat{\gamma}_{11} \leq \frac{g_1}{1+\varepsilon g_2}$ and $\Pr\left\{\gamma_{12}^{\text{N}} \geq \widehat{\gamma}_{12}\right\} = 1$. Substituting them in (46) and (47), we have $P_{\text{out},1} = P_{\text{out},2} = 1-\Pr\left\{g_1 \geq \varepsilon\widehat{\gamma}_{11}g_2\right\}$ as $\rho \to \infty$, which can be readily derived as (50). ∎

Following a similar procedure as that of the FRS-N scheme, it can be shown that P_{out}^{∞} decreases monotonically with decreasing $\widehat{\gamma}_{11}$ (or β). Thus, a small $\widehat{\gamma}_{11}$ is suggested for the CRS-N scheme, whereas the allowed minimum $\widehat{\gamma}_{11}$ should be determined considering the practical modulation and coding schemes.

B. CRS-F Scheme

In the CRS-F scheme, RS is employed at U_2 and $\boldsymbol{x}_2$ is split into $\boldsymbol{x}_{21}$ and $\boldsymbol{x}_{22}$, respectively. At the BS, the decoding order $\boldsymbol{x}_{21} \to \boldsymbol{x}_1 \to \boldsymbol{x}_{22}$ is applied. Regarding the decoding order, the power allocation factor is implemented to satisfy the QoS requirements $\gamma_{21}^{\text{F}} \geq \widehat{\gamma}_{21}$, $\gamma_1^{\text{F}} \geq \widehat{\gamma}_1$, and $\gamma_{22}^{\text{F}} \geq \widehat{\gamma}_{22}$, sequentially.

Following a similar procedure as that of the CRS-N scheme, the power allocation factor of the CRS-F scheme can be derived as

$$\alpha = \begin{cases} \max(\widehat{\alpha}_{_F}, \widetilde{\alpha}_{_F}), & \widehat{\gamma}_{21} \leq \frac{\varepsilon g_2}{1+g_1} \text{ and } \widehat{\gamma}_1 \leq g_1, \\ \text{does not exist}, & \text{otherwise}, \end{cases} \quad (51)$$

where

$$\widehat{\alpha}_{_F} = \frac{\widehat{\gamma}_{21}}{1+\widehat{\gamma}_{21}}\left(1+\frac{1+g_1}{\varepsilon g_2}\right) \quad (52)$$

and

$$\widetilde{\alpha}_{_F} = \max\left(0, 1-\frac{g_1-\widehat{\gamma}_1}{\varepsilon\widehat{\gamma}_1 g_2}\right). \quad (53)$$

Considering the above power allocation and decoding order $\boldsymbol{x}_{21} \to \boldsymbol{x}_1 \to \boldsymbol{x}_{22}$, the outage probabilities of U_1 and U_2 achieved by the CRS-F scheme can be expressed as

$$P_{\text{out},1} = 1 - \Pr\left\{\left(\widehat{\gamma}_{21} \leq \tfrac{\varepsilon g_2}{1+g_1}\right) \cap \left(\widehat{\gamma}_1 \leq g_1\right)\right\} \quad (54)$$

and

$$P_{\text{out},2} = 1-\Pr\Big\{\left(\widehat{\gamma}_{21} \leq \tfrac{\varepsilon g_2}{1+g_1}\right)\cap\left(\widehat{\gamma}_1 \leq g_1\right)\cap\left(\widehat{\alpha}_{_F} \geq \widetilde{\alpha}_{_F}\right) \cap\left(\gamma_{22}^{\text{F}}(\widehat{\alpha}_{_F}) \geq \widehat{\gamma}_{22}\right)\Big\} - \Pr\Big\{\left(\widehat{\gamma}_{21} \leq \tfrac{\varepsilon g_2}{1+g_1}\right) \cap\left(\widehat{\gamma}_1 \leq g_1\right)\cap\left(\widehat{\alpha}_{_F} < \widetilde{\alpha}_{_F}\right)\cap\left(\gamma_{22}^{\text{F}}(\widehat{\alpha}_{_F}) \geq \widehat{\gamma}_{22}\right)\Big\}, \quad (55)$$

respectively.

Theorem 4. *For the CRS-F scheme, the outage probabilities of U_1 and U_2 are given by*

$$P_{\text{out},1} = 1 - \frac{e^{-\frac{\widehat{\gamma}_{21}}{\varepsilon\rho}}}{\Gamma(N_1)} \sum_{n=0}^{N_2-1}\sum_{k=0}^{n} \frac{\varepsilon^{N_1+k}\rho^k}{n!}\left(\frac{\widehat{\gamma}_{21}}{\varepsilon\rho}\right)^n\binom{n}{k} \times(\varepsilon+\widehat{\gamma}_{21})^{-N_1-k}\Gamma\left(N_1+k, \tfrac{\widehat{\gamma}_1}{\rho}\left(1+\tfrac{\widehat{\gamma}_{21}}{\varepsilon}\right)\right) \quad (56)$$

and

$$P_{\text{out},2} = 1 - \frac{e^{-\frac{\widehat{\gamma}_{21}+\widehat{\gamma}_{22}+\widehat{\gamma}_{21}\widehat{\gamma}_{22}}{\varepsilon\rho}}}{\Gamma(N_1)} \sum_{n=0}^{N_2-1}\sum_{k=0}^{n} \frac{\varepsilon^{N_1+k}\rho^k}{n!}\left(\frac{\widehat{\gamma}_{21}}{\varepsilon\rho}\right)^n \times\binom{n}{k}\left(\frac{\widehat{\gamma}_{21}+\widehat{\gamma}_{22}+\widehat{\gamma}_{21}\widehat{\gamma}_{22}}{\widehat{\gamma}_{21}}\right)^{n-k}(\varepsilon+\widehat{\gamma}_{21})^{-N_1-k} \times\Gamma\left(N_1+k, \tfrac{\widehat{\gamma}_1(1+\widehat{\gamma}_{22})}{\rho}\left(1+\tfrac{\widehat{\gamma}_{21}}{\varepsilon}\right)\right), \quad (57)$$

respectively.

Proof: A proof for Theorem 4 is similar to that of Theorem 3 and omitted here to save space. ∎

Proposition 4. *As $\rho \to \infty$, asymptotic outage probabilities of U_1 and U_2 achieved by the CRS-F scheme are the same, which is given by*

$$P_{\text{out}}^{\infty} = 1-\frac{1}{\Gamma(N_1)} \sum_{n=0}^{N_2-1} \frac{\Gamma(N_1+n)}{n!}\left(\frac{\widehat{\gamma}_{21}}{\varepsilon}\right)^n\left(1+\frac{\widehat{\gamma}_{21}}{\varepsilon}\right)^{-N_2-n}. \quad (58)$$

Proof: As $\rho \to \infty$, we have an asymptotic expression $\widehat{\gamma}_{21} \leq \frac{\varepsilon g_2}{g_1}$ for $\widehat{\gamma}_{21} \leq \frac{\varepsilon g_2}{g_1}$. In addition, we have $\Pr\left\{\widehat{\gamma}_1 \leq g_1\right\} = 1$ and $\Pr\left\{\gamma_{22}^{\text{F}} \geq \widehat{\gamma}_{22}\right\} = 1$, so that $P_{\text{out},1} = P_{\text{out},2} = P_{\text{out}}^{\infty} = 1 - \Pr\left\{g_2 \geq \widehat{\gamma}_{21}g_1/\varepsilon\right\}$ as $\rho \to \infty$. With the aid of the PDF and CDF of F_{g_i}, P_{out}^{∞} can be derived as (58). ∎

As such, it can be shown that P_{out}^{∞} decreases monotonically with decreasing $\widehat{\gamma}_{21}$ and a small β is suggested for the CRS-F scheme.

V. Simulation Results

In this section, we present Monte Carlo simulation results to verify the outage performance achieved by the proposed RS schemes. In the simulation, we set $B = 64$ and $N_c = 6$ for the CP-SC transmission and apply $\rho = \bar{P}_1/\sigma^2$ denoting the equivalent SNR. In all figures, the results achieved by the conventional uplink NOMA with the SIC processing are denoted by NOMA.

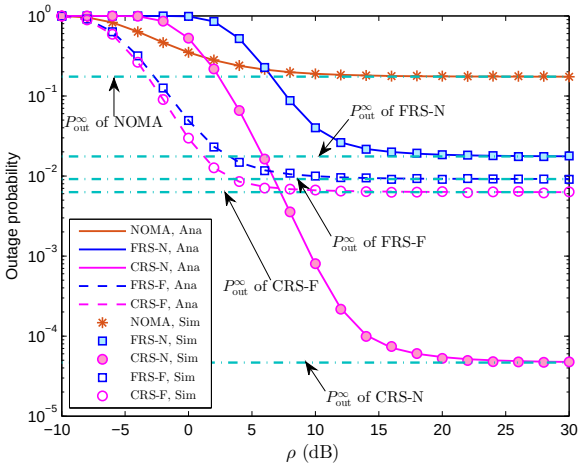

(a) Outage probability of U_1.

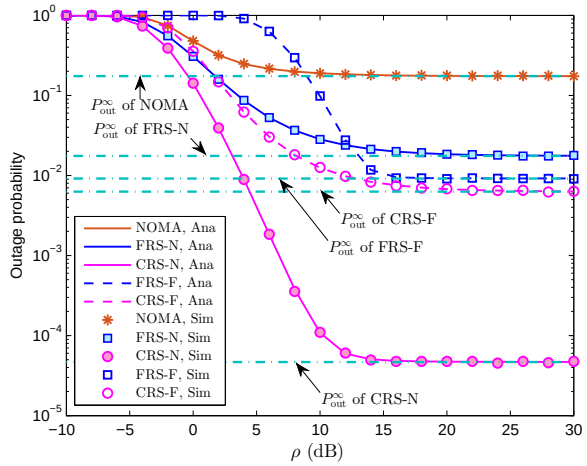

(b) Outage probability of U_2.

Fig. 3. Outage probability versus SNR.

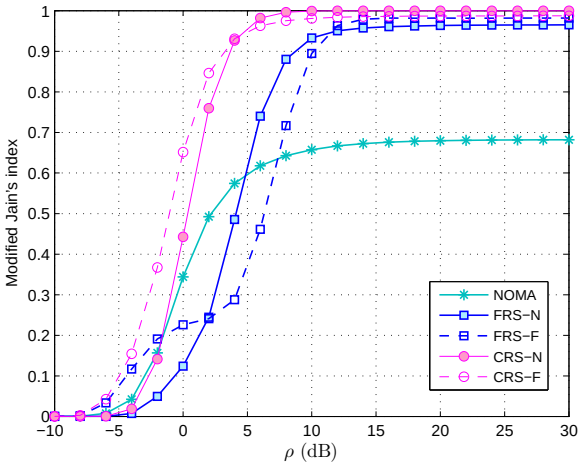

Fig. 4. Modified Jain's index versus SNR.

In Fig. 3, the outage probability versus SNR is investigated. For the simulation corresponding to this figure, we set $N_1 = N_2 = 4$, $m = 4$, $\widehat{R}_1 = \widehat{R}_2 = 1.0$ bps/Hz, and $\varepsilon = -3$ dB. For the FRS-N and FRS-F schemes, we set $\alpha = 0.9$ and $\beta = 0.1$. The results in Fig. 3(a) and Fig. 3(b) show that the proposed FRS and CRS schemes significantly

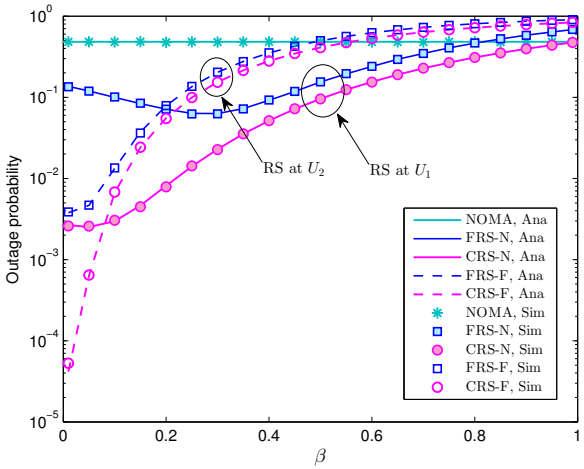

Fig. 5. Outage probability versus RS factor ($\rho = 10$ dB).

decrease the outage probabilities for both U_1 and U_2 in the middle and high SNR regions. Moreover, the results in Fig. 3(a) and Fig. 3(b) verify the correctness of the analytical outage probability expressions for all the considered schemes. In Fig. 3(a), the FRS-F scheme achieves the smaller outage probability for U_1 than that of the FRS-N scheme in the considered whole SNR region. The reason is that less error propagation is encountered for the detection of $\boldsymbol{x}_1$ when RS is applied at the far user. Similarly, the CRS-F scheme achieves the smaller outage probability than that of the CRS-N scheme for U_1 in the low SNR region. However, in the middle and high SNR regions, the CRS-F scheme achieves the larger outage probability than that of the CRS-N scheme due to the fact that the outage probabilities in the middle and high SNR regions are mainly determined by γ_{12}^{N} and γ_1^{F} for the CRS-N and CRS-F schemes, respectively, and we always have $\gamma_{12}^{\text{N}} > \gamma_1^{\text{F}}$. It is worthy pointing out that both the FRS-N and CRS-N schemes achieve the larger outage probabilities for U_1 than that of the "NOMA" scheme in the low SNR region due to error propagation in SIC processing. However, in the middle and high SNR regions, both the FRS-N and CRS-N schemes can decrease the outage probabilities significantly and the CRS-N achieves the lowest outage probability among all the schemes. Conclusively, to achieve the lowest outage probability for U_1, the CRS-F scheme should be applied in the low SNR region, whereas the CRS-N scheme should be applied in the middle and high SNR regions.

In Fig. 3(b), the results show that the FRS-N, CRS-N, and CRS-F schemes achieve the smaller outage probabilities for U_2 than that of "NOMA" in the considered whole SNR region. Only the FRS-F scheme achieves the larger outage probability for U_2 than that of "NOMA" in the small SNR region due to error propagation for the detection of $\boldsymbol{x}_2$ when RS is applied at the far user. In contrast, when RS is applied at the near user, the CRS-N scheme achieves the smallest outage probability for U_2 among all the schemes due to less error propagation for the detection of $\boldsymbol{x}_2$ besides the PA in the cognitive way. Therefore, to achieve the best outage performance for U_2, the CRS-N scheme should be applied in the considered whole SNR region.

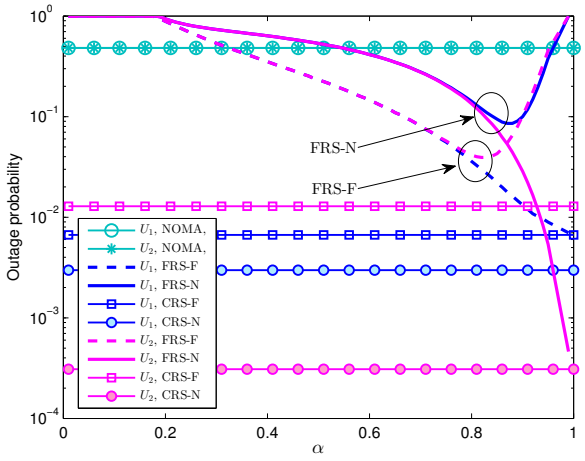

Fig. 6. Outage probability versus power allocation factor ($\rho = 10$ dB).

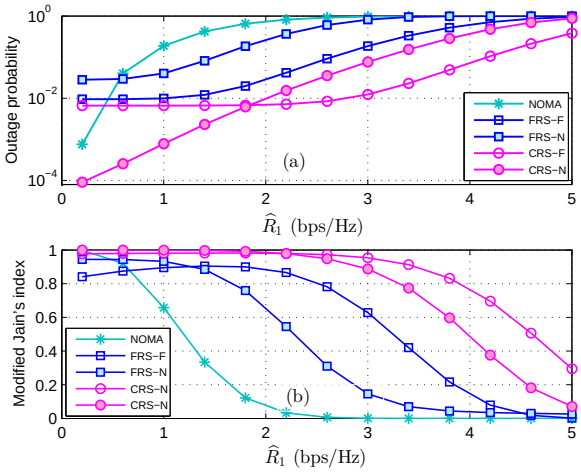

Fig. 7. Outage probability and fairness versus $\widehat{R}_1$ (fixed $\widehat{R}_2 = 1$ bps/Hz).

Regading the system parameters of Fig. 3, the user fairness versus SNR is investigated in Fig. 4. In this figure, it is observed that the modified Jain's index increases for all the schemes with an increasing SNR. In the middle and high SNR regions, all the FRS schemes outperform NOMA on the modified Jain's index. For FRS-N and CRS-N schemes, the achieved modified Jain's indices are smaller than that of NOMA only in the low SNR region. For FRS-F and CRS-F schemes, thpe achieved modified Jain's indices are larger than that of NOMA in the low SNR region. Only in the middle SNR region, the modified Jain's index achieved by the FRS-F scheme is smaller than that of NOMA. Moreover, in Fig. 4, it is illustrated that the CRS-F scheme achieves the best fairness in the low SNR region, whereas the CRS-N scheme attains the best fairness in the middle and high SNR regions. Conclusively, the proposed FRS schemes achieve better fairness than that of NOMA.

In Fig. 5, we investigate the impact of the RS factor on the outage probabilities of all the RS schemes. In the simulation corresponding to this figure, we set $N_1 = N_2 = 4$, $m = 4$, $\widehat{R}_1 = 1.5$ bps/Hz, $\widehat{R}_2 = 1.0$ bps/Hz, $\varepsilon = -3$ dB, and $\rho = 10$ dB. For the FRS-N and FRS-F schemes, we also set $\alpha = 0.9$. Since a larger β results in the larger $\widehat{\gamma}_{11}$ and $\widehat{\gamma}_{21}$ for the detections of $\boldsymbol{x}_{11}$ and $\boldsymbol{x}_{21}$, respectively, increasing β can be regarded as increasing error propagation in SIC processing equivalently. Note that the results for U_2 is similar to that for U_1, we only plot the results for U_1 in Fig. 5. In this figure, the outage probabilities achieved by NOMA for U_1 are larger than 0.1 since NOMA cannot detect the desired signals under the considered SNR $\rho = 10$ dB. In the small and middle β regions, where the effect of error propagation is weak, all the proposed RS schemes achieve the smaller outage probabilities for U_1, respectively. When RS is applied at the near user U_1, the results in Fig. 5 show that the outage probabilities achieved by the FRS-N and CRS-N for U_1 first decrease with increasing β, which indicate that strong channel gain of the near user can support the correct detection of $\boldsymbol{x}_{11}$; then, the outage probabilities increase after β approaches a threshold value, which indicates that error propagation dominates the detection performance of SIC processing. When RS is applied at the far user U_2, the outage probabilities achieved by the FRS-F and CRS-F schemes always increase with increasing β. Moreover, in the small β region, where the effect of error propagation is weak, the FRS-F and CRS-F schemes achieve the smaller outage probabilities for U_1 than those of the FRS-N and CRS-N schemes, respectively. However, in the middle and large β regions, where $\widehat{\gamma}_{11}$ and $\widehat{\gamma}_{21}$ are relatively large, the outage performance are mainly determined by whether $\boldsymbol{x}_{11}$ and $\boldsymbol{x}_{21}$ can be detected correctly. Consequently, the FRS-N and CRS-N schemes achieve the smaller outage probabilities than those of the FRS-F and CRS-F schemes, respectively, due to the strong channel gain associated with U_1. Moreover, all the RS schemes cannot correctly detect the desired signals in the high β region, where the corresponding target rates $\widehat{\gamma}_{11}$ and $\widehat{\gamma}_{21}$ are too high to be satisfied. In summary, β should be set to be a smaller value such that the effect of error propagation is weak. In addition, we note that the CRS-F and CRS-N schemes should be applied to achieve the lowest outage probabilities for U_1 and U_2, respectively.

In Fig. 6, we investigate the impact of the power allocation factor on the outage performance for the FRS-N and FRS-F schemes, respectively, with the system parameters $N_1 = N_2 = 4$, $m = 4$, $\widehat{R}_1 = 1.5$ bps/Hz, $\widehat{R}_2 = 1.0$ bps/Hz, $\beta = 0.1$, and $\rho = 10$ dB. For the FRS-N and FRS-F schemes, we increase α from 0.01 to 0.99. Recalling that the decoding order $\boldsymbol{x}_{11} \rightarrow \boldsymbol{x}_2 \rightarrow \boldsymbol{x}_{12}$ is applied in the FRS-N scheme, increasing α always increases γ_{11}^{N} and γ_2^{N}, so that the detection performance of $\boldsymbol{x}_{11}$ and $\boldsymbol{x}_2$ can be improved. Consequently, the outage probability of U_2 achieved by the FRS-N scheme always decreases with increasing α. Although increasing α increases γ_{11}^{N} and γ_2^{N}, the corresponding decreased γ_{12}^{N} cannot ensure the correct detection of $\boldsymbol{x}_{12}$ when α surpasses a threshold value. Therefore, the outage probability of U_1 achieved by the FRS-N scheme first decreases with increasing α; then, the outage probability increases with increasing α after α approaches a threshold value. The similar phenomenon also occurs for the FRS-F scheme, i.e., the outage probability of U_1 always decreases with increasing α due to the increased γ_{21}^{F} and γ_1^{F} considering that the decoding order $\boldsymbol{x}_{21} \rightarrow \boldsymbol{x}_1 \rightarrow \boldsymbol{x}_{22}$ is applied in the FRS-F scheme. In contrast, the outage prob-

ability of U_2 achieved by the FRS-F scheme first decreases with increasing α; then, it increases with increasing α after α surpasses a threshold value. Therefore, when the FRS-F and FRS-N schemes are applied, α should be chosen to guarantee a desirable outage performance for both users. Moreover, the curves in Fig. 6 show that the CRS-N scheme achieves the smallest outage probabilities for U_1 and U_2 under the considered system parameters. In addition, the CRS-F scheme achieves the smaller outage probabilities for U_1 and U_2 than those of "NOMA" , respectively. It is worthy pointing out that the power allocation factors of the CRS-N and CRS-F schemes are adaptively determined by (44) and (51), respectively, which do not increases from 0.01 to 0.99 as that in the simulation for the FRS-N and FRS-F scheme.

In Fig. 7, the impacts of targeted transmit rate on outage probability and fairness are investigated with the system parameter $N_1 = N_2 = 4$, $m = 4$, $\varepsilon = 3$ dB, and $\rho = 10$ dB. Moreover, we set a fixed target rate $\widehat{R}_2 = 1$ bps/Hz and increase the target rate $\widehat{R}_1$ from 0.2 bps/Hz to 5 bps/Hz. Without loss of generality, only the outage probability of U_1 is presented in Fig. 7(a), while and the modified Jain's index versus $\widehat{R}_1$ is plotted in Fig. 7(b). According to the curves in Fig. 7(a), the outage probability of U_1 achieved by NOMA increases quickly with increasing $\widehat{R}_1$; after $\widehat{R}_1$ surpasses a threshold value, the outage probability of U_1 reaches 1. For U_1, the results in Fig. 7(a) show that the outage probabilities achieved by the FRS-F, FRS-N, and CRS-F schemes are smaller than that of NOMA in the middle and high $\widehat{R}_1$ regions, respectively. Moreover, the CRS-N scheme always achieves the smaller outage probability than that of NOMA in the considered whole $\widehat{R}_1$ region. However, the CRS-F achieves the smaller outage probability than that of the CRS-N scheme in the middle and high $\widehat{R}_1$ regions.

The results in Fig. 7(b) show that the FRS-N, FRS-F, and CRS-N schemes achieve the larger modified Jain's indices than that of NOMA in the middle and high $\widehat{R}_1$ regions, respectively. With increasing $\widehat{R}_1$, the modified Jain's indices achieved by the FRS-N, CRS-F, and CRS-N schemes decrease accordingly. In contrast, the modified Jain's index achieved by the FRS-F scheme first increases with an increasing $\widehat{R}_1$. After $\widehat{R}_1$ surpasses a threshold, the modified Jain's index achieved by the FRS-F scheme decreases with an increasing $\widehat{R}_1$. Moreover, the CRS-F scheme achieves the largest modified Jain's index almost in the considered whole $\widehat{R}_1$ region. Thus, the proposed RS scheme provides the better fairness over that of NOMA.

VI. Conclusions

In this paper, we have investigated the FRS and CRS schemes for the uplink NOMA over frequency selective fading channels. Employing fixed power allocation and cognitive power allocation, both the FRS and CRS schemes have been applied at the near and far user, respectively, which significantly improve the outage performance and user fairness. Closed-form expressions for the outage probabilities of both users have been derived for the FRS and CRS schemes, respectively. The benefits of applying RS to improve the user fairness and outage performance have been revealed. It has been shown that the CRS-N scheme achieves the best outage performance for both users in the middle and high SNR regions. The superior outage performance and the enhanced user fairness achieved by the proposed FRS and CRS schemes over that of NOMA have been corroborated by Monte Carlo simulation results.

Appendix A: A proof of Theorem 1

Considering that any unsuccessful detecting of $\boldsymbol{x}_{11}$, $\boldsymbol{x}_2$, and $\boldsymbol{x}_{12}$ will result in an outage event for detecting $\boldsymbol{x}_1$, a non-outage event regarding detecting $\boldsymbol{x}_1$ only occurs when $\boldsymbol{x}_{11}$, $\boldsymbol{x}_2$, and $\boldsymbol{x}_{12}$ are all detected successfully. Thus, the outage probability of U_1 in (24) can be rewritten as

$$P_{\text{out},1} = 1-\Pr\left\{(\gamma_{11}^{\text{N}} \geq \widehat{\gamma}_{11}) \cap (\gamma_2^{\text{N}} \geq \widehat{\gamma}_2) \cap (\gamma_{12}^{\text{N}} \geq \widehat{\gamma}_{12})\right\}. \quad \text{(A.1)}$$

After some algebraic manipulations, (A.1) can be expressed as

$$P_{\text{out},1} = 1-\Pr\Bigg\{(g_1 > \tau) \cap\Big(\tfrac{(1-\alpha)\widehat{\gamma}_2 g_1}{\varepsilon} + \tfrac{\widehat{\gamma}_2}{\varepsilon} \leq g_2 \leq \tfrac{g_1}{\varepsilon\tau_2} - \tfrac{1}{\varepsilon}\Big)\Bigg\}, \quad \text{(A.2)}$$

where $\tau \triangleq \max\{\tau_1, \tau_2, \tau_3\}$, $\tau_1 \triangleq \frac{\widehat{\gamma}_{12}}{1-\alpha}$, $\tau_2 \triangleq \frac{\widehat{\gamma}_{11}}{\alpha-(1-\alpha)\widehat{\gamma}_{11}}$, $\tau_3 \triangleq \frac{(1+\widehat{\gamma}_2)\widehat{\gamma}_{11}}{\alpha-(1-\alpha)(1+\widehat{\gamma}_2)\widehat{\gamma}_{11}}$, and $g_i \triangleq \rho||\boldsymbol{h}_i||^2$ is the equivalent channel gain, which follows a chi-squared distribution with $2N_i$ degrees of freedom and a scale constant ρ. Then, $P_{\text{out},1}$ can be evaluated as

$$P_{\text{out},1} = 1-\int_{\tau}^{\infty}\left(F_{g_2}\left(\tfrac{x}{\varepsilon\tau_2} - \tfrac{1}{\varepsilon}\right) - F_{g_2}\left(\tfrac{(1-\alpha)\widehat{\gamma}_2 x}{\varepsilon} + \tfrac{\widehat{\gamma}_2}{\varepsilon}\right)\right) \times f_{g_1}(x)\mathrm{d}x, \quad \text{(A.3)}$$

where $f_{g_i}(\cdot)$ and $F_{g_i}(\cdot)$ are the PDF and CDF of g_i, respectively [1]. By using [54, Eq. (1.111)], (A.3) can be further evaluated as $P_{\text{out},1} = 1 - I_1 + I_2$, where I_1 and I_2 are given by (26) and (27), respectively.

The outage probability of U_2 in (25) can be rewritten as

$$P_{\text{out},1} = 1 - \Pr\left\{(\gamma_{11}^{\text{N}} \geq \widehat{\gamma}_{11}) \cap (\gamma_2^{\text{N}} \geq \widehat{\gamma}_2)\right\}. \quad \text{(A.4)}$$

After some mathematical manipulation, (A.4) can be expressed as

$$\begin{aligned} P_{\text{out},2} &= 1-\Pr\left\{(g_1 > \tau_2) \cap \left(\tfrac{(1-\alpha)\widehat{\gamma}_2 g_1}{\varepsilon} + \tfrac{\widehat{\gamma}_2}{\varepsilon} \leq g_2 \leq \tfrac{g_1}{\varepsilon\tau_2} - \tfrac{1}{\varepsilon}\right)\right\} \\ &= 1-\int_{\tau_2}^{\infty}\left(F_{g_2}\left(\tfrac{x}{\varepsilon\tau_2} - \tfrac{1}{\varepsilon}\right) - F_{g_2}\left(\tfrac{(1-\alpha)\widehat{\gamma}_2 x}{\varepsilon} + \tfrac{\widehat{\gamma}_2}{\varepsilon}\right)\right) \times f_{g_1}(x)\mathrm{d}x. \end{aligned} \quad \text{(A.5)}$$

Then, (A.5) can be evaluated as $P_{\text{out},2} = 1 - I_3 + I_4$, where I_3 and I_4 are given by (28) and (29), respectively.

APPENDIX B: A PROOF OF THEOREM 3

After some mathematical manipulation, the outage probability of U_1 in (46) can be rewritten as

$$\begin{aligned}P_{\text{out},1} &= 1-\Pr\left\{\left(g_2 > \tfrac{\widehat{\gamma}_2(1+\widehat{\gamma}_{12})}{\varepsilon}\right) \cap \left(\varepsilon\widehat{\gamma}_{11}g_2 + \widehat{\gamma}_{11} + \widehat{\gamma}_{12}\right.\right. \\ &\quad \left.\left. + \widehat{\gamma}_{11}\widehat{\gamma}_{21} < g_1 \leq \tfrac{\varepsilon g_2(1+\widehat{\gamma}_{11}+\widehat{\gamma}_{11}\widehat{\gamma}_{12})}{\widehat{\gamma}_2} - 1\right)\right\} - \Pr\left\{\right. \\ &\quad \left.\left(g_2 > \tfrac{\widehat{\gamma}_2(1+\widehat{\gamma}_{12})}{\varepsilon}\right) \cap \left(g_1 > \tfrac{\varepsilon g_2(1+\widehat{\gamma}_{11}+\widehat{\gamma}_{11}\widehat{\gamma}_{12})}{\widehat{\gamma}_2} - 1\right)\right\} \\ &= 1 - \Pr\left\{\left(g_2 > \tfrac{\widehat{\gamma}_2(1+\widehat{\gamma}_{12})}{\varepsilon}\right) \cap \left(g_1 > \varepsilon\widehat{\gamma}_{11}g_2 + \widehat{\gamma}_{11}\right.\right. \\ &\quad \left.\left. + \widehat{\gamma}_{12} + \widehat{\gamma}_{11}\widehat{\gamma}_{21}\right)\right\} \\ &= 1 - \int_{\frac{\widehat{\gamma}_2(1+\widehat{\gamma}_{12})}{\varepsilon}}^{\infty} \left(1 - F_{g_1}(\varepsilon\widehat{\gamma}_{11} + \widehat{\gamma}_{11} + \widehat{\gamma}_{12} + \widehat{\gamma}_{11}\widehat{\gamma}_{21})\right) \\ &\quad \times f_{g_2}(x)\mathrm{d}x. \end{aligned} \tag{B.1}$$

Using [54, Eq. (1.111)], the above expression can be further evaluated as (48).

For U_2, the outage probability in (47) can be expressed as

$$\begin{aligned}P_{\text{out},2} &= 1 - \Pr\left\{\left(g_2 > \widehat{\gamma}_2/\varepsilon\right) \cap \left(g_1 > \varepsilon\widehat{\gamma}_{11}g_2 + \widehat{\gamma}_{11}\right)\right\} \\ &= 1 - \int_{\frac{\widehat{\gamma}_2}{\varepsilon}}^{\infty} \left(1 - F_{g_1}(\varepsilon\widehat{\gamma}_{11}x + \widehat{\gamma}_{11})\right) f_{g_2}(x)\mathrm{d}x, \end{aligned} \tag{B.2}$$

which can be evaluated as (49) with the aid of [54, Eq. (1.111)].

REFERENCES

[1] H. Liu, T. A. Tsiftsis, K. S. Kwak, , and H. V. Poor, "Rate splitting for asynchronous uplink NOMA systems with cyclic prefixed single carrier," in *Proc. IEEE International Conference on Communications (ICC) Workshops*, Shanghai, China, 20-24 May 2019, pp. 1–6.

[2] S. M. R. Islam, N. Avazov, O. A. Dobre, and K. S. Kwak, "Power-domain non-orthogonal multiple access (NOMA) in 5G systems: Potential and challenges," *IEEE Commun. Surv. Tut.*, vol. 19, no. 2, pp. 721–742, 2nd Quarter 2017.

[3] Y. Liu, Z. Qin, M. Elkashlan, Z. Ding, A. Nallanathan, and L. Hanzo, "Non-orthogonal multiple access for 5G and beyond," *Proc. IEEE*, vol. 105, no. 12, pp. 2347–2381, Dec. 2017.

[4] A. Kiani and N. Ansari, "Edge computing aware NOMA for 5G networks," *IEEE Internet Things J.*, vol. 5, no. 2, pp. 1299–1306, Apr. 2018.

[5] T. M. Cover, "Broadcast channels," *IEEE Trans. Inf. Theory*, vol. 18, no. 1, pp. 2–14, Jan. 1972.

[6] A. Wyner, "Recent results in the Shannon theory," *IEEE Trans. Inf. Theory*, vol. 20, no. 1, pp. 2–10, Jan. 1974.

[7] R. Gallager, "An inequality on the capacity region of multiple access multipath channels," in *Communications and Cryptography: Two Sides and One Tapestry*, pp. 129–139, Kluwer, 1994.

[8] Z. Ding, Z. Yang, P. Fan, and H. V. Poor, "On the performance of non-orthogonal multiple access in 5G systems with randomly deployed users," *IEEE Signal Process. Lett.*, vol. 21, no. 12, pp. 1501–1505, Dec. 2014.

[9] Z. Wei, J. Guo, D. W. K. Ng, and J. Yuan, "Fairness comparison of uplink NOMA and OMA," in *Proc. 2017 IEEE 85th Vehicular Technology Conference (VTC-Spring)*, Sydney, NSW, Australia, 4-7 Jun. 2017, pp. 1–6.

[10] S. Timotheou and I. Krikidis, "Fairness for non-orthogonal multiple access in 5G systems," *IEEE Signal Process. Lett.*, vol. 22, no. 10, pp. 1647–1651, Oct. 2015.

[11] Y. Endo, Y. Kishiyama, and K. Higuchi, "Uplink non-orthogonal access with MMSE-SIC in the presence of inter-cell interference," in *Proc. 2012 Int. Symp. Wireless Commun. Syst. (ISWCS)*, Paris, France, 28-31 Aug. 2012, pp. 261–265.

[12] M. Mollanoori and M. Ghaderi, "Uplink scheduling in wireless networks with successive interference cancellation," *IEEE Trans. Mobile Comput.*, vol. 13, no. 5, pp. 1132–1144, May 2014.

[13] X. Chen, A. Benjebbour, A. Li, and A. Harada, "Multi-user proportional fair scheduling for uplink non-orthogonal multiple access (NOMA)," in *Proc. IEEE Vehicular Technology Conference (VTC-Spring)*, Seoul, South Korea, 18-21 May 2014, pp. 1–5.

[14] M. Al-Imari, P. Xiao, M. A. Imran, and R. Tafazolli, "Uplink non-orthogonal multiple access for 5G wireless networks," in *Proc. 11th Int. Symp. Wireless Commun. Syst. (ISWCS)*, Barcelona, Spain, 26-29 Aug. 2014, pp. 781–785.

[15] L. Lei, D. Yuan, C. K. Ho, and S. Sun, "Power and channel allocation for non-orthogonal multiple access in 5G systems: Tractability and computation," *IEEE Trans. Wireless Commun.*, vol. 15, no. 12, pp. 8580–8594, Dec. 2016.

[16] F. Guo, H. Lu, D. Zhu, and Z. Gu, "Joint user association, grouping and power allocation in uplink noma systems with qos constraints," in *Proc. IEEE International Conference on Communications (ICC)*, Shanghai, China, 20-24 May 2019, pp. 1–6.

[17] M. Pischella and D. Le Ruyet, "NOMA-relevant clustering and resource allocation for proportional fair uplink communications," *IEEE Wireless Commun. Lett.*, vol. 8, no. 3, pp. 873–876, Jun. 2019.

[18] G. Gui, H. Sari, and E. Biglieri, "A new definition of fairness for non-orthogonal multiple access," *IEEE Commun. Lett.*, vol. 23, no. 7, pp. 1267–1271, July 2019.

[19] N. Zhang, J. wang, G. Kang, and Y. Liu, "Uplink non-orthogonal multiple access in 5G systems," *IEEE Communi. Lett.*, vol. 20, no. 3, pp. 458–461, Mar. 2016.

[20] Z. Yang, Z. Ding, P. Fan, and N. Al-Dhahir, "A general power allocation scheme to guarantee quality of service in downlink and uplink NOMA systems," *IEEE Trans. Wireless Commun.*, vol. 15, no. 11, pp. 7244–7257, Nov. 2016.

[21] Y. Liu, M. Derakhshani, and S. Lambotharan, "Outage analysis and power allocation in uplink non-orthogonal multiple access systems," *IEEE Commun. Lett.*, vol. 22, no. 2, pp. 336–339, Feb. 2018.

[22] E. Balevi and R. D. Gitlin, "Pareto optimization for uplink NOMA power control," in *Proc. 2018 Wireless Telecommunications Symposium (WTS)*, Phoenix, AZ, USA, 17-20 April 2018, pp. 1–5.

[23] E. Balevi, "Multiuser diversity gain in uplink NOMA," in *Proc. IEEE 88th Vehicular Technology Conference (VTC-Fall)*, Chicago, IL, USA, 27-30 Aug. 2018, pp. 1–5.

[24] Y. Gao, B. Xia, K. Xiao, Z. Chen, X. Li, and S. Zhang, "Theoretical analysis of the dynamic decode ordering SIC receiver for uplink NOMA systems," *IEEE Commun. Lett.*, vol. 21, no. 10, pp. 2246–2249, Oct. 2017.

[25] Z. Zhang and R. Q. Hu, "Uplink non-orthogonal multiple access with fractional power control," in *Proc. 2017 IEEE Wireless Communications and Networking Conference (WCNC)*, San Francisco, CA, USA, 19-22 Mar. 2017, pp. 1–6.

[26] Y. Liu, M. Derakhshani, and S. Lambotharan, "Outage analysis and power allocation in uplink non-orthogonal multiple access systems," *IEEE Commun. Lett.*, vol. 22, no. 2, pp. 336–339, Mar. 2018.

[27] B. Clerckx, H. Joudeh, C. Hao, M. Dai, and B. Rassouli, "Rate splitting for MIMO wireless networks: a promising PHY-layer strategy for LTE evolution," *IEEE Commun. Mag.*, vol. 54, no. 5, pp. 98–105, May 2016.

[28] H. Joudeh and B. Clerckx, "Rate-splitting for max-min fair multigroup multicast beamforming in overloaded systems," *IEEE Trans. Wireless Commun.*, vol. 16, no. 11, pp. 7276–7289, Nov. 2017.

[29] A. R. Flores, B. Clerckx, and R. C. de Lamare, "Energy efficiency of rate-splitting multiple access, and performance benefits over SDMA and NOMA," in *Proc. 15th ISWCS*, Lisbon, Portugal, 28-31 Aug. 2018, pp. 1–6.

[30] Y. Mao, B. Clerckx, and V. O. K. Li, "Rate-splitting multiple access for coordinated multi-point joint transmission," in *Proc. IEEE International Conference on Communications (ICC) Workshops*, Shanghai, China, 20-24 May 2019, pp. 1–6.

[31] T. Han and K. Kobayashi, "A new achievable rate region for the interference channel," *IEEE Trans. Inf. Theory*, vol. 27, no. 1, pp. 49–60, Jan. 1981.

[32] H. Dahrouj and W. Yu, "Multicell interference mitigation with joint beamforming and common message decoding," *IEEE Trans. Commun.*, vol. 59, no. 8, pp. 2264–2273, Aug. 2011.

[33] C. Hao, Y. Wu, and B. Clerckx, "Rate analysis of two-receiver MISO broadcast channel with finite rate feedback: A rate-splitting approach," *IEEE Trans. Commun.*, vol. 63, no. 9, pp. 3232–3246, Sept. 2015.

[34] M. Dai, B. Clerckx, D. Gesbert, and G. Caire, "A rate splitting strategy for massive MIMO with imperfect CSIT," *IEEE Trans. Wireless Commun.*, vol. 15, no. 7, pp. 4611–4624, July 2016.

[35] Y. Mao, B. Clerckx, and V. O. K. Li, "Rate-splitting for multi-antenna non-orthogonal unicast and multicast transmission," in *Proc. IEEE 19th SPAWC*, Kalamata, Greece, 25-28 Jun. 2018, pp. 1–5.

[36] B. Zheng, F. Chen, M. Wen, Q. Li, Y. Liu, and F. Ji, "Secure NOMA based cooperative networks with rate-splitting source and full-duplex relay," in *Proc. 2018 15th International Symposium on Wireless Communication Systems (ISWCS)*, Lisbon, Portugal, 28-31 Aug. 2018, pp. 1–5.

[37] Y. Mao, B. Clerckx, and V. O. K. Li, "Rate-splitting for multi-user multi-antenna wireless information and power transfer," in *Proc. IEEE 20th SPAWC*, Cannes, France, 2-5 July 2019, pp. 1–5.

[38] B. Rimoldi and R. Urbanke, "A rate-splitting approach to the Gaussian multiple-access channel," *IEEE Trans. Inf. Theory*, vol. 42, no. 2, pp. 364–375, Mar. 1996.

[39] D. Tse and P. Viswanath, *Fundamentals of Wireless Communication*. Cambridge, U.K.: Cambridge Univ. Press, 2005.

[40] Y. Zhu, Z. Zhang, X. Wang, and X. Liang, "A low-complexity non-orthogonal multiple access system based on rate splitting," in *Proc. 2017 9th International Conference on Wireless Communications and Signal Processing (WCSP)*, Nanjing, China, 11-13 Oct. 2017, pp. 1–6.

[41] J. Zeng, T. lv, W. Ni, R. Liu, N. C. Beaulieu, and Y. J. G. Fan, "Ensuring max-min fairness of UL SIMO-NOMA: A rate splitting approach," *IEEE Trans. Veh. Technol.*, In Press, 2019.

[42] Y. Zhu, X. Wang, Z. Zhang, X. Chen, and Y. Chen, "A rate-splitting non-orthogonal multiple access scheme for uplink transmission," in *Proc. 2017 9th International Conference on Wireless Communications and Signal Processing (WCSP)*, Nanjing, China, 11-13 Oct. 2017, pp. 1–6.

[43] I. Baig, "A precoding-based multicarrier non-orthogonal multiple access scheme for 5G cellular networks," *IEEE Access*, vol. 5, pp. 19 233–19 238, Oct. 2017.

[44] X. Zou, B. He, and H. Jafarkhani, "On uplink asynchronous non-orthogonal multiple access systems with timing error," in *2018 IEEE International Conference on Communications (ICC)*, Kansas City, MO, USA, 20-24 May 2018, pp. 1–6.

[45] X. Wang, F. Labeau, and L. Mei, "Asynchronous uplink non-orthogonal multiple access (NOMA) with cyclic prefix," in *Proc. 2018 IEEE Wireless Communications and Networking Conference (WCNC)*, Barcelona, Spain, 15-18 Apr. 2018, pp. 1–6.

[46] D. Falconer, S. L. Ariyavisitakul, A. Benyamin-Seeyar, and B. Eidson, "Frequency domain equalization for single-carrier broadband wireless systems," *IEEE Commun. Mag.*, vol. 40, no. 4, pp. 58–66, Apr. 2002.

[47] S. Ohno, "Performance of single-carrier block transmissions over multipath fading channels with linear equalization," *IEEE Trans. Signal Process.*, vol. 54, no. 10, pp. 3678–3687, Oct. 2006.

[48] S. G. Larew, T. A. Thomas, M. Cudak, and A. Ghosh, "Air interface design and ray tracing study for 5G millimeter wave communications," in *Proc. IEEE GLOBECOM Workshops*, Atlanta, GA, USA, 9-13 Dec. 2013, pp. 117–122.

[49] H. Nikopour, W. Lee, R. Doostnejad, E. Sasoglu, C. D. Silva, H. Niu, and S. Talwar, "Single carrier waveform solution for millimeter wave air interface," in *Proc. GLOBECOM Workshops*, Washington, DC, USA, 4-8 Dec. 2016, pp. 1–6.

[50] K. J. Kim, M. D. Renzo, H. Liu, P. V. Orlik, and H. V. Poor, "Performance analysis of distributed single carrier systems with distributed cyclic delay diversity," *IEEE Trans. Commun.*, vol. 65, no. 12, pp. 5514–5528, Dec. 2017.

[51] K. J. Kim and T. A. Tsiftsis, "On the performance of cyclic prefix-based single-carrier cooperative diversity systems with best relay selection," *IEEE Trans. Wireless Commun.*, vol. 10, no. 4, pp. 1269–1279, Apr. 2011.

[52] M. Vaezi and H. V. Poor, "Simplified han-kobayashi region for one-sided and mixed Gaussian interference channels," in *Proc. IEEE International Conference on Communications (ICC)*, Kuala Lumpur, Malaysia, 22-27 May 2016, pp. 1–6.

[53] Z. Ding, P. Fan, and H. V. Poor, "Impact of user pairing on 5G nonorthogonal multiple-access downlink transmissions," *IEEE Trans. Veh. Technol.*, vol. 65, no. 8, pp. 6010–6023, Aug. 2016.

[54] I. S. Gradshteyn and I. M. Ryzhik, *Table of Integrals, Series, and Products*. New York: Academic Press, 2007.